NATIONAL TECHNICAL UNIVERSITY OF ATHENS
SCHOOL OF ELECTRICAL AND COMPUTER ENGINEERING
SCHOOL OF MECHANICAL ENGINEERING

INTERDISCIPLINARY POSTGRADUATE PROGRAMME
“Translational Engineering in Health and Medicine”

TITLE
“EMG Analysis of Redundant and Synergistic Muscle Coordination and Cross-Frequency Coupling During Grip Force Control”

Postgraduate Diploma Thesis

Postgraduate student Karolina Ronzi

Supervisor: Dr Ioannis Delis, Assistant Professor, School of Biomedical Sciences, University of Leeds

Athens, October 2025

NATIONAL TECHNICAL UNIVERSITY OF ATHENS
SCHOOL OF ELECTRICAL AND COMPUTER ENGINEERING
SCHOOL OF MECHANICAL ENGINEERING

INTERDISCIPLINARY POSTGRADUATE PROGRAMME
"Translational Engineering in Health and Medicine"

TITLE
"EMG Analysis of Redundant and Synergistic Muscle Coordination and Cross-Frequency Coupling During Grip Force Control"

Postgraduate Diploma Thesis

Postgraduate student Karolina Ronzi

Supervisor: Dr Ioannis Delis, Assistant Professor, School of Biomedical Sciences, University of Leeds

The postgraduate diploma thesis has been approved by the examination committee on*:*
29 October 2025

1st member	*2nd member*	*3rd member*
Dr Ioannis Delis, Assistant Professor, University of Leeds, School of Biomedical Sciences	Dr Konstantina Nikita, Professor, NTUA, School of Electrical and Computer Engineering	Athanasios Rontogiannis, Associate Professor, NTUA, School of Electrical and Computer Engineering

Athens*,*October 2025

Karolina Ronzi
Graduate of the Interdisciplinary Postgraduate Programme,
“Translational Engineering in Health and Medicine”,
Master of Science,
School of Electrical and Computer Engineering,
National Technical University of Athens

This research is dedicated to my family and the people who inspired this journey and believed in it before I did.

ABSTRACT

Understanding how the central nervous system coordinates synergistic and redundant muscle activations to achieve stable and adaptable movement remains a central question in motor neuroscience. This study investigates the structure of redundant and synergistic muscle coordination during grip force control and explores the modulation of high-frequency electromyographic activity by low-frequency oscillations, with cross-frequency coupling. Using EMG recordings from upper-limb muscles during object-lifting tasks, we applied an information-theoretic framework to decompose muscle interactions into redundant and synergistic components based on mutual information metrics. These metrics quantified how pairs of muscles shared or complemented task-relevant information about grip force. Non-negative matrix tri-factorization was used to extract low-dimensional spatial and temporal synergy modules. The analysis revealed that muscle redundancy was negligible, while spatial synergy typically featured one primary muscle exhibiting strong coordination with multiple others. Although the dominant synergistic muscle varied across participants, the deltoid consistently showed high synergy. Temporal synergy was more diverse and most pronounced during the early phase of grip control.

Phase-amplitude coupling analysis was conducted to investigate whether low-frequency EMG phase modulated high-frequency amplitude, reflecting potential shared neural drives. Initial PAC estimation using Hilbert-transform based filtering without surrogates indicated modulation centered around a 2 Hz phase frequency, possibly influenced by trial alignment. A subsequent analysis using Morlet wavelet convolution with surrogate normalization revealed more individualized PAC patterns, where the most modulating phase frequency varied across participants. For each participant, two EMG channels were selected based on synergy strength, and a composite channel was formed by averaging their activity to represent a synergistic unit. Correlations between grip force and the three PAC measures were examined, along with synergy-grip force correlations. The deltoid-dominated channel exhibited the highest, though not statistically significant, correlation with grip force.

These findings suggest that low-frequency oscillations modulate high-frequency EMG activity in a muscle and participant-specific manner and that both synergy and PAC may encode shared neural drives related to grip force control. Limitations include the restricted participant subset used for PAC, those with high synergy values, selective channel analysis, and the use of a simple averaging method to generate composite synergy signals. Future work should refine composite signal computation and directly relate PAC and synergy to enhance predictive modeling of physiological outcomes.

Keywords: Electromyography, Motor Coordination, Redundant Muscle Activation, Synergistic Muscle Activation, Mutual Information, Grip Force Control, Spatial Synergy, Temporal Synergy, Phase-Amplitude Coupling, Modulation Index

ACKNOWLEDGEMENTS

I would like to express my deepest gratitude to my supervisor, Dr. Ioannis Delis, Assistant Professor at the School of Biomedical Sciences, University of Leeds, for his guidance, and encouragement throughout the course of this thesis. His expertise and support have been invaluable in shaping this research.

I am also sincerely thankful to my co-supervisor, Dr. Konstantina Nikita, Professor at the School of Electrical and Computer Engineering, National Technical University of Athens, for her mentorship.

Special thanks are due to Kyriakos Birmpas PhD candidate, for his technical assistance, practical advice, and constant willingness to help during this study.

This work was carried out within the framework of the Interdisciplinary Postgraduate Programme "Translational Engineering in Health and Medicine" of NTUA, Greece. I am grateful for the academic environment and resources provided by the programme, which made this research possible.

Finally, I would like to thank my family and friends for their continuous encouragement, understanding, and support throughout my studies.

TABLE OF CONTENTS

LIST OF FIGURES

LIST OF TABLES

LIST OF ABBREVIATIONS

AD	Anterior Deltoid
BI	Biceps Brachii
BR	Brachioradialis
CFC	Cross-Frequency Coupling
Ch1, Ch2	First and second EMG channels selected for each participant, based on the strongest spatial synergy values
CNS	Central Nervous System
EEG	Electroencephalography
EMG	Electromyography
FE	Finger Extensors
Fs	Sampling Frequency
GPU	Graphics Processing Unit
Hz	Hertz
LD	Latissimus Dorsi
MEG	Magnetoencephalography
MI (Information Theory)	Mutual Information- quantifies dependence between muscle activations
MI (PAC)	Modulation Index- quantifies phase-amplitude coupling strength
NIF	Network Information Framework
NMF	Non-negative Matrix Factorization
NTUA	National Technical University of Athens
PAC	Phase-Amplitude Coupling
PD	Posterior Deltoid

PE	Pectoralis Major
ROI	Region of Interest
sEMG	Surface Electromyography
sNM3F	Sample-based Non-negative Matrix Tri-Factorization
TM	Medial Triceps
TL	Lateral Triceps
2D	Two-Dimensional
z-score	Standardized Score

CHAPTER 1

AIM OF THE STUDY

The primary aim of this study is to characterize how redundant and synergistic patterns of muscle coordination contribute to grip force control and to examine their relationship with cross-frequency coupling mechanisms in electromyography signals. Specifically, the study seeks to quantify redundant and synergistic interactions between upper-limb muscles during a precision grip task using an information-theoretic framework based on mutual information decomposition. Spatiotemporal muscle synergies are extracted and visualized using non-negative matrix tri-factorization to identify low-dimensional coordination modules underlying grip force generation. Phase-amplitude coupling is assessed within individual and synergistic muscle signals to determine whether the phase of low-frequency oscillations modulates the amplitude of high-frequency EMG activity during grip force control. Finally, synergy and PAC measures are correlated to grip force metrics to investigate whether slow oscillatory components of EMG signals reflect shared neural drives that modulate muscle activation during grip force control. Through this approach, the study aims to contribute to the quantitative understanding of how muscle coordination and oscillatory coupling relate to grip force control.

CHAPTER 2

INTRODUCTION

2.1 Motor Control and Synergy

Motor control is a highly coordinated process in which the central nervous system organizes muscle activity into low-dimensional modules known as *muscle synergies*. The synergy hypothesis, first proposed by Nikolai Bernstein (1967), argues that the CNS simplifies control by activating groups of muscles as functional units rather than independently. This modular control reduces the complexity of managing redundant degrees of freedom in movement.

Bizzi et al. (2008) demonstrated that spinal circuits encode a limited set of activation patterns that can be linearly combined to produce diverse motor behaviors, forming the modern basis of the synergy framework. Similarly, d'Avella and Bizzi (2005) used electromyography (EMG) data to show consistent muscle coordination modules across movements, suggesting that synergies are stable representations of motor tasks. Ting and McKay (2007) further proposed that these synergies are adaptable, allowing for dynamic control of posture and balance through differential recruitment of overlapping modules.

Recent findings support a hierarchical organization of synergies, integrating both spatial and temporal components of muscle coordination (Zhao et al., 2024; Luo et al., 2024). These results confirm that muscle synergies reflect an underlying structure of neural control that optimizes efficiency, and adaptability in motor performance.

2.2 EMG Signal Processing

Surface electromyography (sEMG) serves as the principal method for recording the electrical activity underlying muscle activation. EMG signals capture the summation of motor unit action potentials, providing a non-invasive window into neuromuscular coordination. The correct interpretation of EMG requires preprocessing, including rectification, bandpass filtering, normalization, and envelope extraction, to isolate physiologically meaningful information.

De Luca (1997) outlined foundational guidelines for EMG acquisition and analysis, emphasizing the importance of minimizing cross-talk and electrode placement errors. Merletti and Farina (2016) extended these principles by introducing advanced methods for spatial EMG decomposition and signal conditioning, which enable the extraction of motor unit firing behavior.

In the context of synergy studies, preprocessing directly influences the number and structure of synergies derived (De Bei, 2025). Filtering choices and signal normalization alter the dimensionality of data used for matrix factorization methods like Non-negative Matrix Factorization (NMF) (Ranaldi et al., 2021). Thus, EMG signal processing is integral to accurate synergy characterization.

2.3 Information Theory in Motor Control

Information theory provides a quantitative framework for understanding how muscles share and distribute neural information during coordinated tasks. *Mutual Information (MI)* is used to measure the statistical dependency between muscle signals, allowing decomposition into redundant, unique, and synergistic contributions (Williams and Beer, 2010).

Delis et al. (2018) introduced an information decomposition framework that applies MI to muscle synergy analysis, distinguishing between shared and complementary information encoded by muscle groups. O'Reilly and Delis (2022) extended this approach using a *network information-theoretic model* to quantify both spatial and temporal synergy structures. These approaches enable a deeper understanding of how distributed motor commands are optimized to maintain stability and adaptability. Recent advances show that redundancy supports perturbation, whereas synergy contributes to flexibility in motor coordination (Chen et al., 2025).

2.4 Matrix Factorization and Synergy Extraction

Non-negative Matrix Factorization (NMF) and its extensions, such as Sample-based Non-negative Matrix Tri-Factorization (Delis, 2014) are computational methods for identifying low-dimensional modules from EMG data. These approaches assume that muscle activations can be represented as the product of spatial (muscle weighting) and temporal (activation pattern) matrices.

Berret and Delis (2018) developed sNM3F to simultaneously extract spatial and temporal modules, offering improved interpretability over traditional NMF. This method captures dynamic patterns that vary across time, allowing insight into how synergies evolve during continuous motor tasks. Ranaldi et al. (2021) validated objective criteria for selecting the appropriate number of synergies, addressing one of the major methodological challenges in the field.

Higher-order extensions, such as tensor decomposition (Ebied, 2019), capture multidimensional interactions across frequency, muscle, and time domains. Such advancements have made synergy extraction more physiologically grounded, supporting applications from motor rehabilitation (Rabbi, 2022) to predictive joint modeling (Xu et al., 2023).

2.5 Cross-Frequency Coupling

Neural oscillations at different frequencies interact through *cross-frequency coupling (CFC)*, where the phase of low-frequency rhythms modulates the amplitude of high-frequency activity. This relationship, quantified through *Phase-Amplitude Coupling (PAC)*, reflects hierarchical neural communication mechanisms.

Canolty et al. (2006) first demonstrated that high-gamma power is modulated by low-frequency theta phase in the human cortex, establishing PAC as a key measure of neural synchronization. Tort et al. (2010) introduced the *Modulation Index (MI)*, a normalized entropy-based measure that quantifies the strength of phase-amplitude relationships.

Florin and Baillet (2015) linked CFC directly to motor control, showing that oscillatory coupling supports sensorimotor integration. In the context of EMG, such coupling can reveal coordination between motor units or across muscles, reflecting shared cortical drives that regulate force and precision (Zhao et al., 2024). These studies form the theoretical foundation for analyzing cross-frequency coupling in muscle activation patterns.

2.6 Hilbert Angle

The Hilbert transform is a classical signal-processing method for obtaining the analytic representation of a real-valued signal. By applying the Hilbert transform $H[x(t)]$, the original signal $x(t)$ can be expressed as a complex analytic signal $z(t)=x(t)+iH[x(t)]$, from which the instantaneous amplitude $A(t)=|z(t)|$ and instantaneous phase $\phi(t)=\arg[z(t)]$ can be directly derived. In the context of phase-amplitude coupling (Tort, 2010), the Hilbert angle approach involves band-pass filtering the signal into two distinct frequency bands, one representing the low-frequency oscillation that provides the phase, and another representing the high-frequency component whose amplitude is modulated by the low-frequency phase. The phase of the low-frequency component and the envelope of the high-frequency component are extracted via the Hilbert transform, and their relationship is quantified using a coupling metric such as the Tort Modulation Index. This method assumes that the narrowband filtering isolates stationary oscillatory components, and that the Hilbert-derived phase angle accurately represents the ongoing oscillatory cycle.

2.7 Morlet Wavelet Convolution

The Morlet wavelet convolution approach (Canolty, R. T. and Knight, R. T. ,2010), (Cohen, M. X., 2014) estimates phase and amplitude by convolving the signal with a family of complex Morlet wavelets, each tuned to a specific center frequency and bandwidth. The wavelet method provides a time-frequency decomposition with adaptive temporal and spectral resolution, capturing transient oscillatory events more precisely than fixed-band Hilbert filters. Unlike the Hilbert approach, which depends on sharply defined band-pass filters, the wavelet-based analytic signal inherently accounts for frequency uncertainty determined by the wavelet's number of cycles. Consequently, the Morlet wavelet PAC estimation is often more sensitive to temporal variability and better suited for analyzing short, nonstationary events such as muscle bursts in EMG recordings. However, this increased flexibility comes with a trade-off in frequency precision relative to the narrowband Hilbert approach.

2.8 Tort Modulation Index

The Tort Modulation Index (MI) is based on the idea that true phase-amplitude coupling leads to a non-uniform distribution of high-frequency amplitudes across the phase of a lower-frequency oscillation. Tort et al. (2010) proposed quantifying this deviation from uniformity by computing the Kullback-Leibler divergence between the observed amplitude-phase distribution and the uniform distribution. The resulting MI is normalized to range between 0 (no coupling) and 1 (maximal coupling). This method provides a measure of PAC that is relatively insensitive to signal amplitude or phase noise, suitable for analyzing both neural and peripheral oscillatory data.

2.9 Clarification on the Meaning of "MI" in Different Analyses

It is important to note that the term MI refers to different quantities in the synergy and PAC analyses. In the synergy and redundancy computations, *MI* denotes Mutual Information, an information-theoretic measure used to quantify the degree of statistical dependence between muscle activation signals. This metric shows how much information about one muscle's activity can be inferred from another, characterizing intermuscular coordination.

In the Phase-Amplitude Coupling (PAC) analysis, *MI* stands for the Modulation Index introduced by Tort et al. (2010). This index measures the strength of coupling between the phase of a low-frequency component and the amplitude of a high-frequency component within the same EMG signal. The Modulation Index reflects the degree to which amplitude fluctuations are organized according to the phase of slower oscillations, and it is unrelated to Mutual Information.

2.10 Linking Synergy and PAC

The integration of synergy analysis and cross-frequency coupling offers a comprehensive perspective on neuromuscular control. While synergy frameworks explain *spatial and temporal coordination* among muscles, cross-frequency coupling describes *temporal modulation and neural synchronization*. Together, they illustrate how the CNS organizes motor output through both modular structure and oscillatory timing.

Delis et al. (2018) and O'Reilly & Delis (2022) provide evidence that mutual information metrics can link synergy activation to temporal oscillations, implying that redundant and synergistic encoding are influenced by rhythmic neural drives. Florin and Baillet (2015) further support this view, showing that cross-frequency coupling between cortical regions correlates with motor performance variability.

Thus, the convergence of these theories suggests that motor coordination emerges from the interaction between modular muscle activation patterns and frequency-specific neural coupling. Understanding this interaction enhances our ability to interpret EMG signals as reflections of hierarchical control mechanisms spanning peripheral and central levels of the motor system.

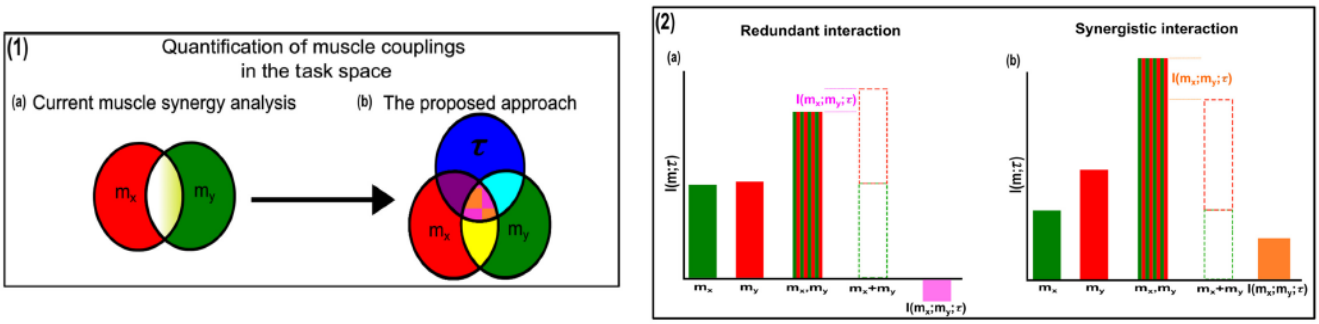

Figure 2.1
Task-synergistic, and task-redundant muscle coordination (by O'Reilly and Delis, 2024)

2.11 Experimental Overview

The study by O'Reilly and Delis (2024) investigated the functional organization of upper-limb muscle synergies during goal-directed reaching movements. Participants were instructed to grasp and lift an object equipped with force sensors that continuously recorded grip and load forces applied by the fingers and thumb. The lifting phase required subjects to raise the object vertically to a prescribed height and maintain it steadily for a short period before returning it to the start position. Across trials, objects of different weights were presented in a pseudo-randomized order. Participants sequentially lifted two objects and verbally reported which felt heavier, allowing the analysis of perceptual weight discrimination in parallel with muscle activation patterns.

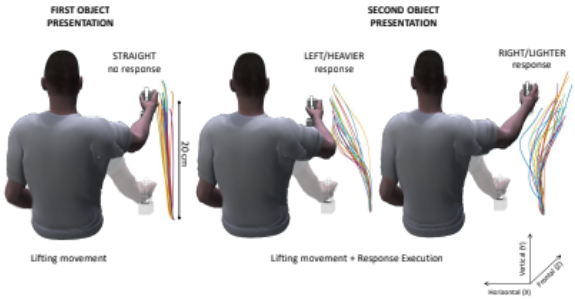

Figure 2.2
Experimental overview
(by Kyriakos Birmpas, 2024)

Surface electromyographic (EMG) signals were recorded from major muscles of the right upper limb, including the finger extensors (FE), brachioradialis (BR), biceps brachii (BI), medial and lateral triceps (TM, TL), anterior and posterior deltoid (AD, PD), pectoralis major (PE), and latissimus dorsi (LD). Each trial consisted of discrete reaching movements executed in both forward and backward directions at controlled velocities. Kinematic data were simultaneously acquired using motion-tracking markers to define task parameters such as endpoint position and movement trajectory.These datasets were processed within the Network Information Framework (NIF) to quantify functional couplings between muscle activity, distinguishing task-redundant, task-synergistic, and task-irrelevant components of motor coordination during the lifting task.

	Muscle	Colour code
1	Opponens Pollicis (Op_Polli)	
2	First Dorsal Interosseous (FDI)	
3	Flexor Carpi Radialis (FlxCarpRad)	
4	Extensor Carpi Radialis (ExtCarpRad)	
5	Upper Trapezius (UpTrap)	
6	Biceps Brachii (BicBrach)	
7	Pectoralis Major (PectMaj)	
8	Anterior Deltoid (AntDel)	
9	Middle Deltoid (MidDel)	

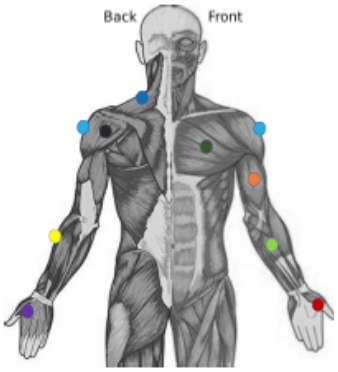

Figure 2.3
Electrode placement
(by Kyriakos Birmpas, 2024)

CHAPTER 3

METHODS AND DATA ANALYSIS

3.1 Grip Force Data Extraction

A MATLAB script was developed to systematically extract and organize the grip force measurements recorded during the experimental sessions for all participants. The original dataset consisted of 22 participant folders, each containing multiple .mat files corresponding to individual experimental trials. Each trial file included a data structure named LiftStrct, which contained nested information about the lifting task, including grip force and stimulus parameters.

All participant data were stored in a directory named DataOutput, with subfolders labeled according to each participant . Each participant folder contained approximately 250 trial files, with file names ending in *newHT.mat. These files included metadata and the relevant trial data. A MATLAB structure named GripForce was initialized with 22 empty fields (Participant1 to Participant22), each representing an individual participant. Each LiftStrct was an array of trials, and within each trial, the field stim held two lift attempts. The grip force signal was stored in the second element of the stim field (stim(2).gripF), which represented the second lift performed by the participant. The extracted grip force signals were stored in a cell array (MGripForce) of size 1×250, corresponding to the maximum number of trials. Each cell contained a vector representing the grip force time series for a given trial.

After processing all valid trials for a participant, the MGripForce cell array was assigned to the respective participant field within the GripForce structure. Once all participant data were processed, the complete structure was saved.This produced a single file (GripForce.mat) containing the grip force measurements for all 22 participants, with each participant's data organized as an independent field for further synchronization and analysis with electromyographic (EMG) data.

3.2 Synergy and Redundancy Analysis Between Muscle Pairs

After extracting the grip force data for each participant, the next step involved quantifying the spatiotemporal synergies and redundancies between pairs of muscles during the grip force task. This analysis aimed to characterize how muscle pairs coordinated their activation patterns to generate the required force output, distinguishing between redundant and synergistic interactions. The electromyographic (EMG) recordings were provided as part of a previously published dataset (O'Reilly & Delis, 2024).

Each participant's EMG data were stored as a cell array containing the time-series recordings from all accepted trials, with muscles represented as columns and time points as rows. For each participant, the EMG signals were first rectified to convert the raw bipolar signals into absolute values, ensuring that both phases of the muscle activity contributed to the overall signal magnitude. The rectified signals were then low-pass filtered at 20 Hz using a 4th-order Butterworth filter to extract the linear envelope; this process isolates the overall activation profile while suppressing high-frequency noise.

Since the duration of individual trials varied, each EMG signal was interpolated and resampled to a uniform length (3500 time points) to ensure comparability across trials. The processed EMG data for each trial were concatenated into a 3D tensor of dimensions [Timepoints × Muscles × Trials], creating the input for the synergy estimation algorithms.

The corresponding grip force time-series were prepared as the task variable, and aligned with the EMG signals using spline interpolation to ensure correspondence between muscle activation and force production.

To estimate the redundant and synergistic components of muscle coordination, the analysis relied on the information decomposition framework developed by (Delis et al., eLife, 2024). Specifically, the MATLAB function SpaceTime_II_Continuous was used to compute mutual information (MI) and co-information between EMG channels and the task variable. The shared and unique information that pairs of muscles contribute to the task, were categorized into redundant interactions (ST_R), where both muscles encode overlapping information about the task, and synergistic interactions (ST_S), where the combination of two muscles provides more task-relevant information than either alone.

To further identify low-dimensional structure in these muscle networks, we used the sample-based Non-negative Matrix Tri-Factorization (sNM3F) algorithm, developed by Berret and Delis (Delis et al., 2018). This algorithm decomposes the muscle-by-time coupling matrices into spatial (Wb) and temporal (Wi) modules. Finally, all synergy-related variables were saved in participant-specific files, containing both the raw coupling matrices and the extracted space-time modules.

3.3 Visualization of Spatial and Temporal Synergy and Redundancy Patterns

Following the computation of the synergy and redundancy matrices for each participant, the next step was visualizing both the spatial and temporal muscle coordination patterns through heatmaps. These heatmaps show how muscles interacted in space and time to contribute to grip force control, distinguishing between cooperative (synergistic) and overlapping (redundant) activity.

All participant-specific outputs from the synergy analysis were stored in MATLAB structures containing the matrices derived from the space-time decomposition and non-negative matrix tri-factorization. The fields gripMI.Wb_S and gripMI.Wb_R contained the spatial synergy and redundancy modules, respectively, while gripMI.ST_S and gripMI.ST_R contained the corresponding temporal synergy and redundancy matrices. These data show the structure of muscle coactivation (spatial domain) and the dynamics of their coordination (temporal domain), for each participant.

A MATLAB script was implemented to automatically generate heatmaps for all four modules. For each of the 22 participants, the script extracted the appropriate matrix. The matrices were reshaped using the squareform function to obtain symmetrical representations, where both axes corresponded to the same set of variables-either individual muscles or discrete time windows. To avoid duplication across the matrix diagonal, only unique pairwise relationships were displayed.

The resulting matrices were visualized using imagesc, with color intensity indicating the strength of synergy or redundancy between variables. Spatial heatmaps displayed pairwise muscle-muscle relationships, groups of muscles that co-activated either synergistically (complementary contributions) or redundantly (shared encoding). Temporal heatmaps displayed the coordination between time windows within each trial, capturing how muscle activity patterns evolved across time. Each visualization included a color bar for magnitude reference and labeled axes corresponding to muscle indices or time windows.

Consistent high-intensity regions of spatial synergy suggested cooperative activation patterns of muscle groupings involved in force generation, whereas high-intensity regions of temporal synergy reflected the time windows in which these muscle activation patterns unfolded during task execution. The variability observed across participants potentially reflected interindividual differences in muscle coordination strategies or variations in recording quality.

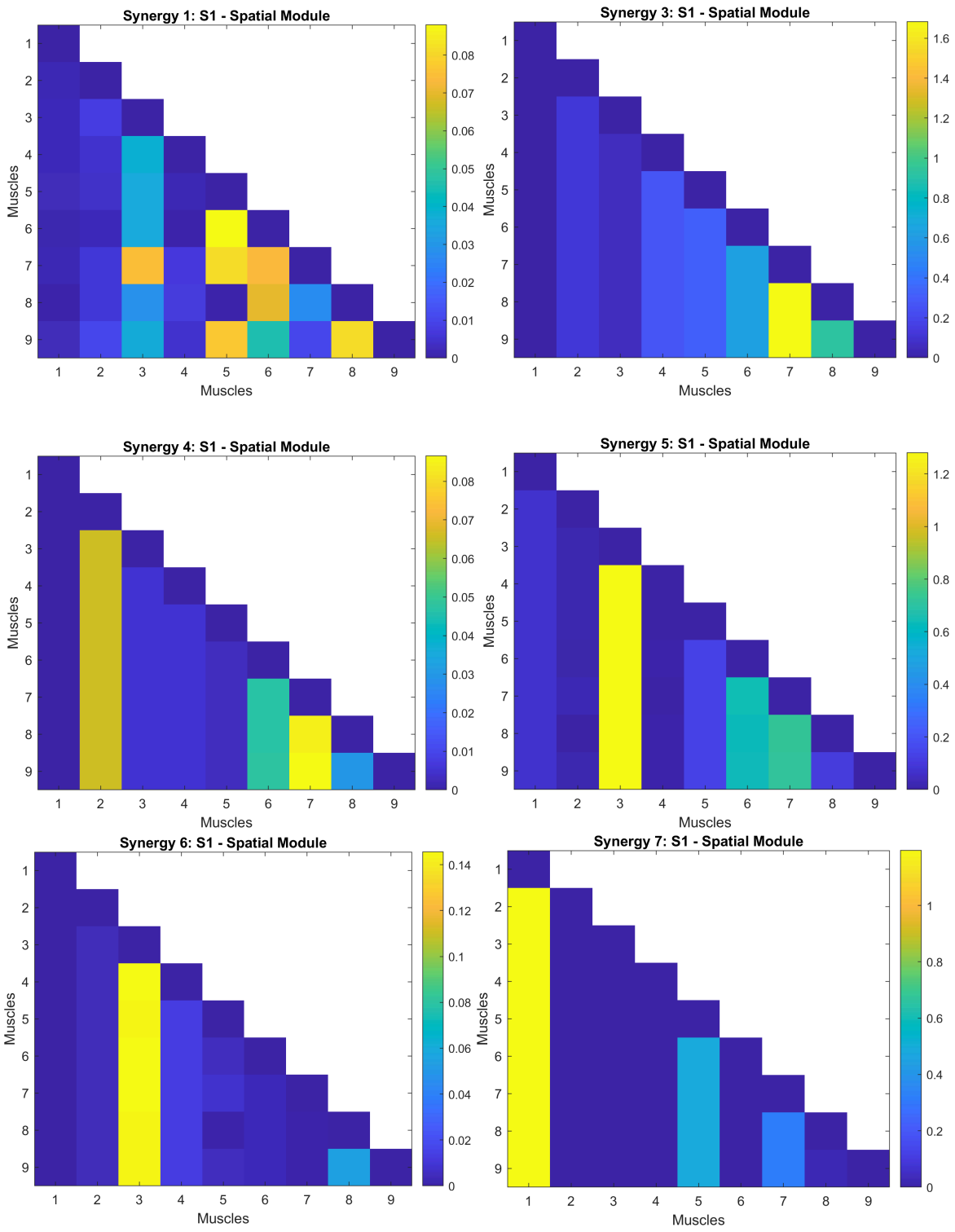

Figure 3.1

Spatial synergy heatmaps for (A) Participant 1; (B) Participant 3; (C) Participant 4; (D) Participant 5; (E) Participant 6; (F) Participant 7;

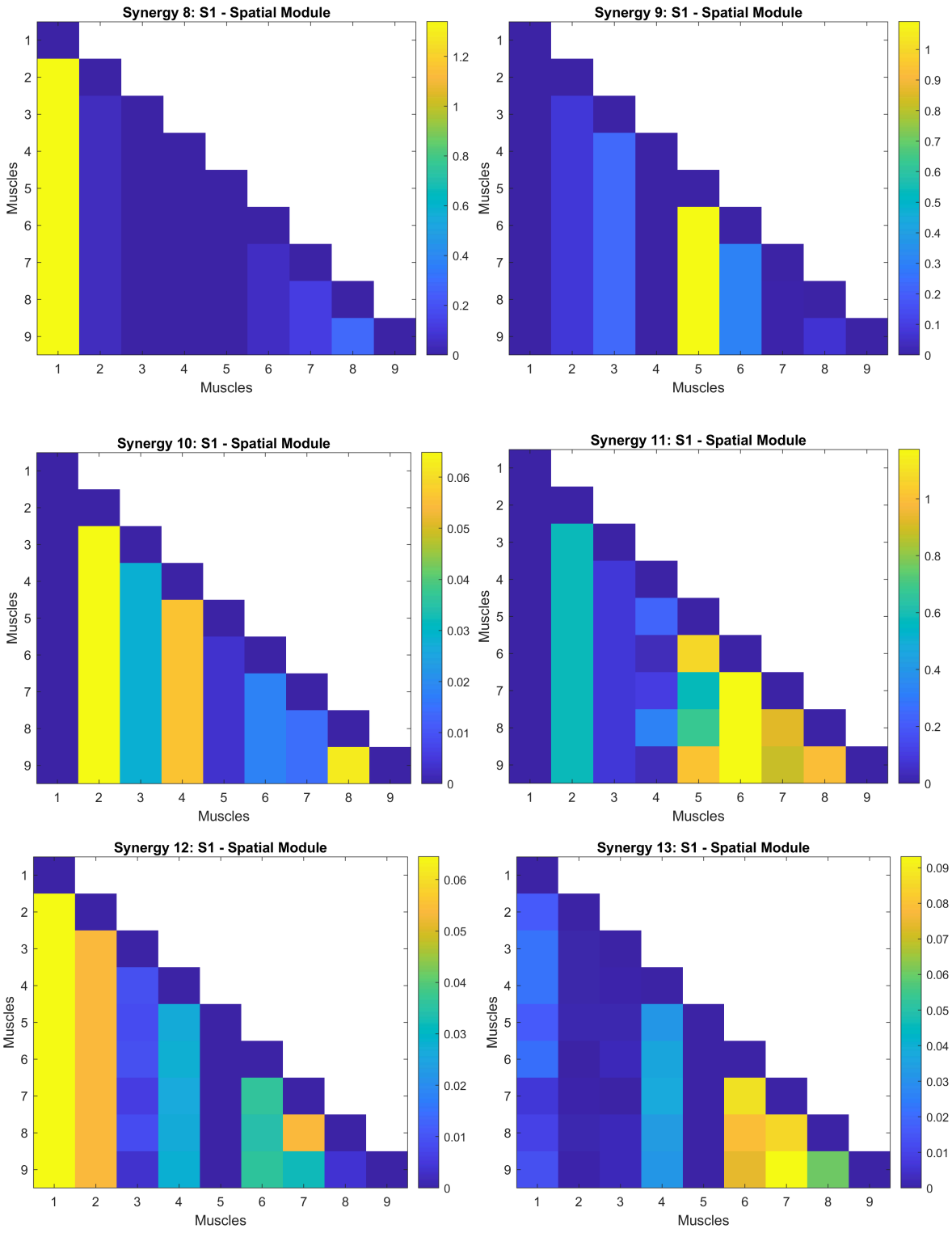

Figure 3.2

Spatial synergy heatmaps for (A) Participant 8; (B) Participant 9; (C) Participant 10; (D) Participant 11; (E) Participant 12; (F) Participant 13;

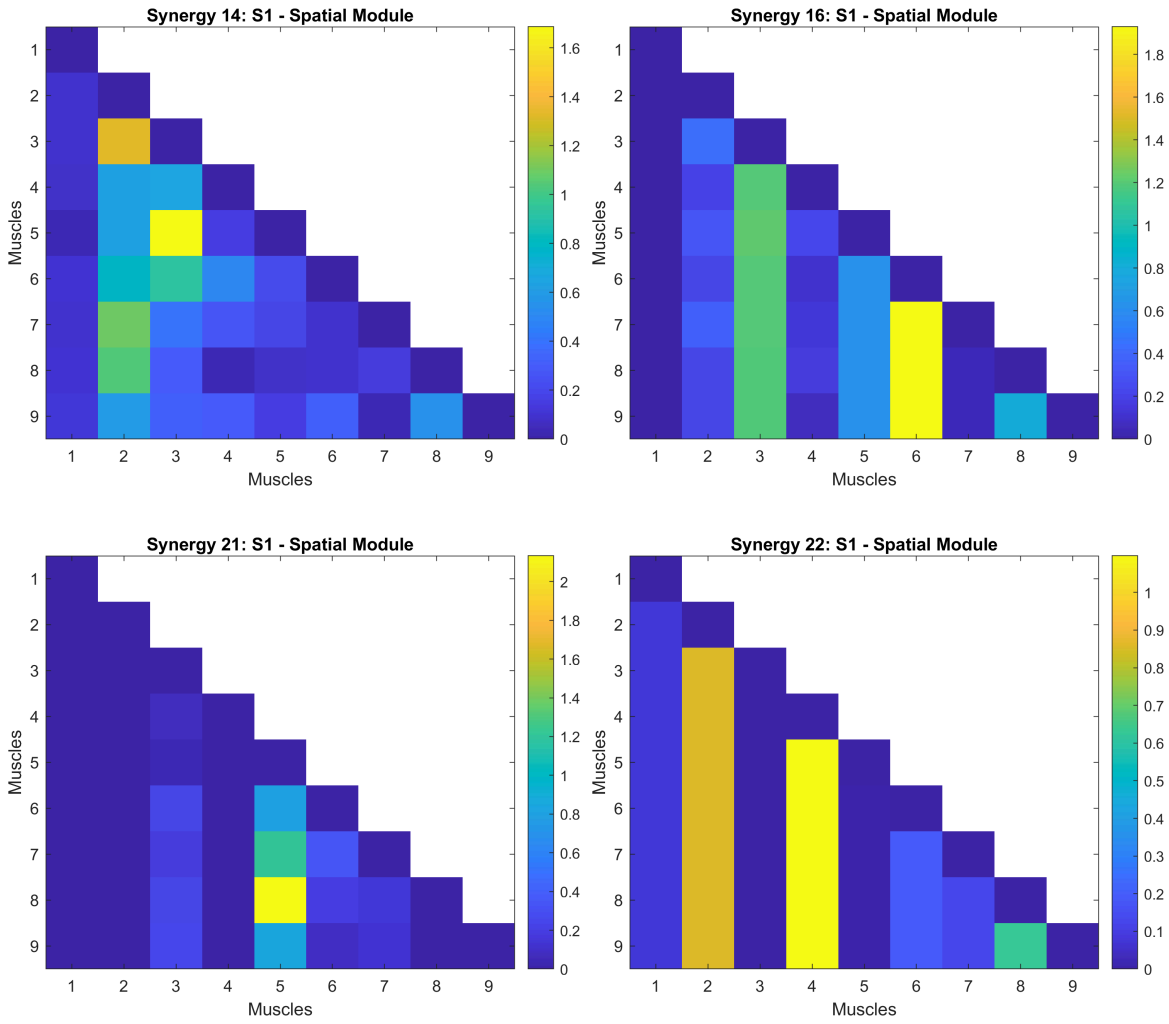

Figure 3.3

Spatial synergy heatmaps for (A) Participant 14; (B) Participant 16; (C) Participant 21; (D) Participant 22;

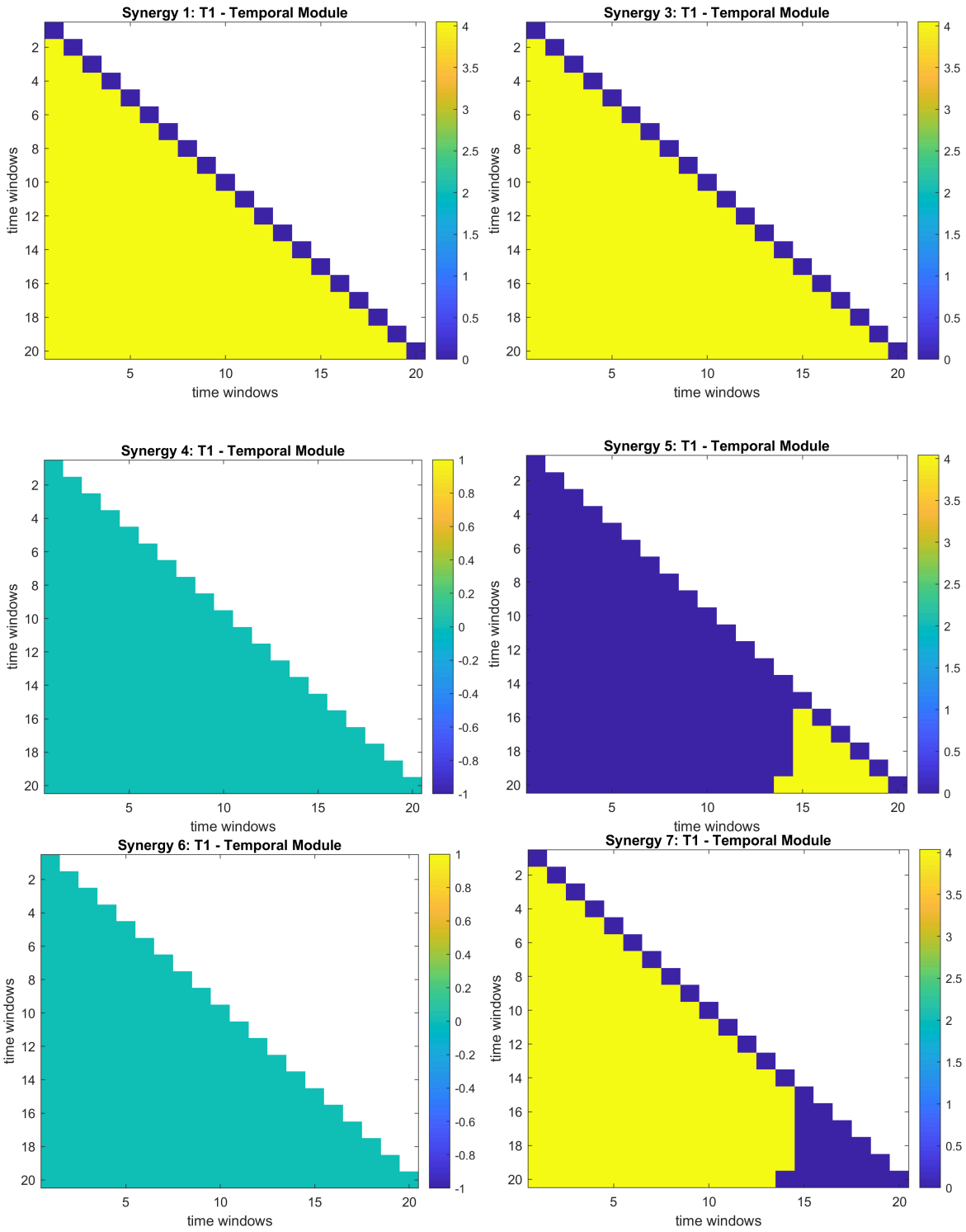

Figure 3.4

Temporal synergy heatmaps for (A) Participant 1; (B) Participant 3; (C) Participant 4; (D) Participant 5; (E) Participant 6; (F) Participant 7;

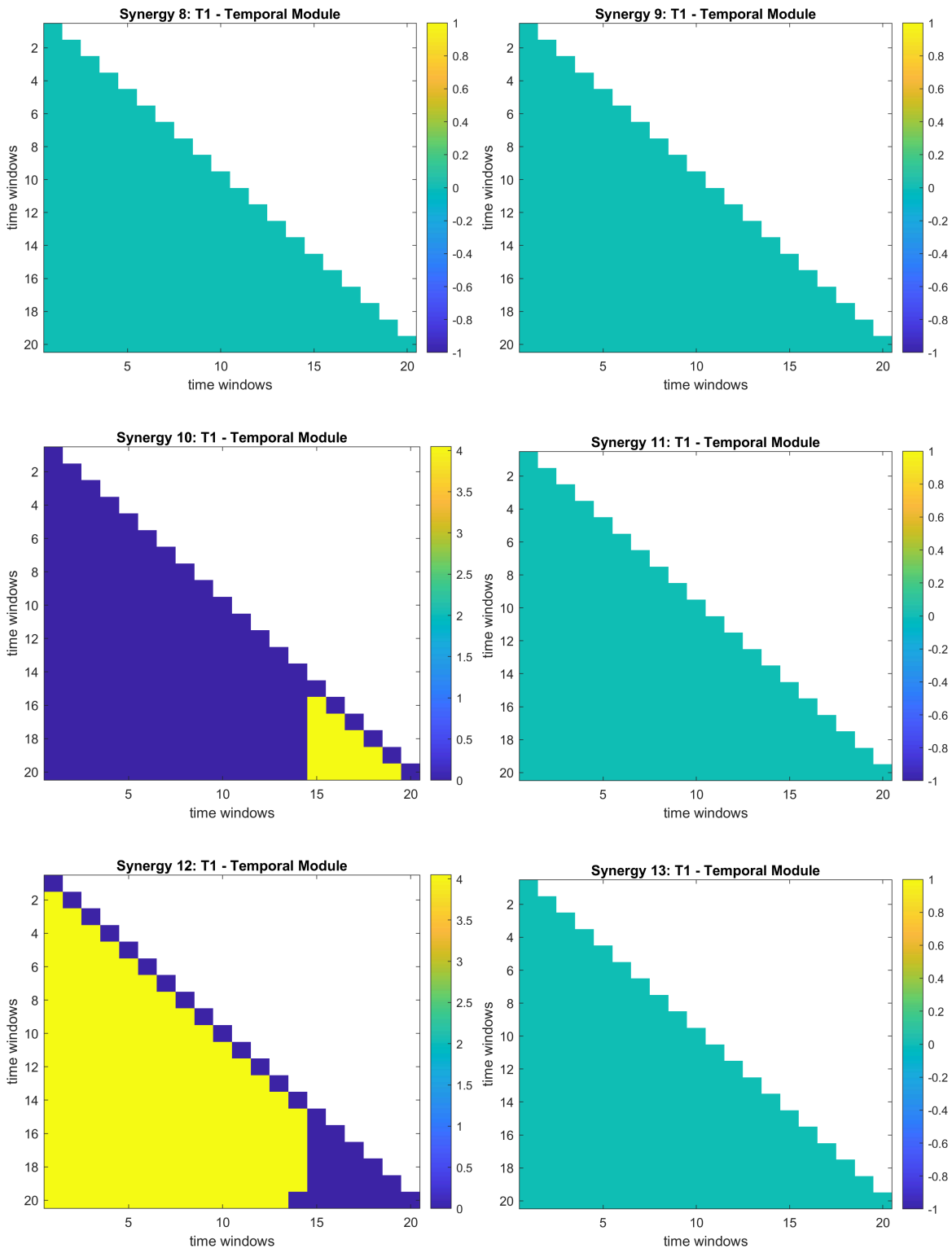

Figure 3.5

Temporal synergy heatmaps for (A) Participant 8; (B) Participant 9; (C) Participant 10; (D) Participant 11; (E) Participant 12; (F) Participant 13;

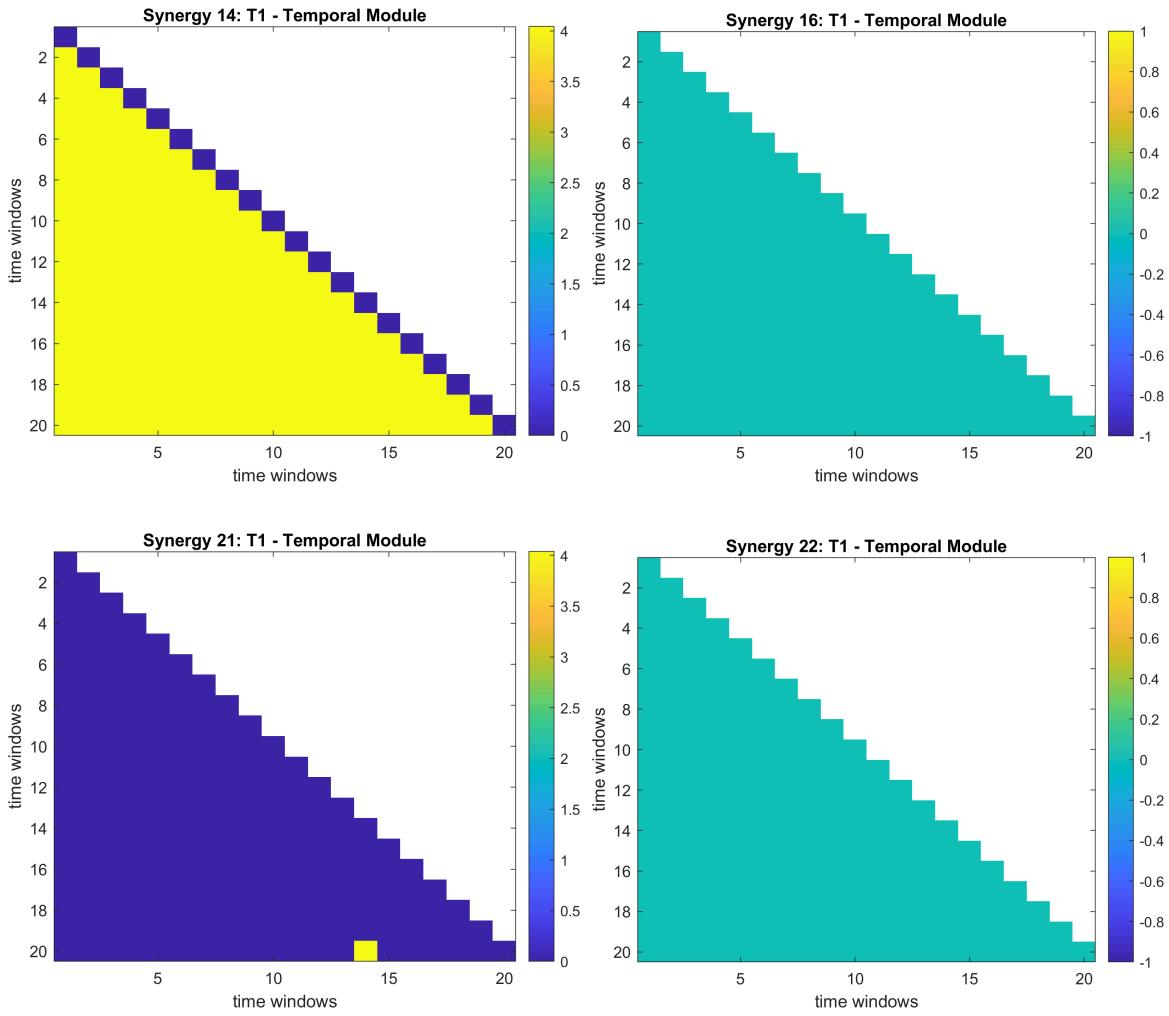

Figure 3.6

Temporal synergy heatmaps for (A) Participant 14; (B) Participant 16; (C) Participant 21; (D) Participant 22;

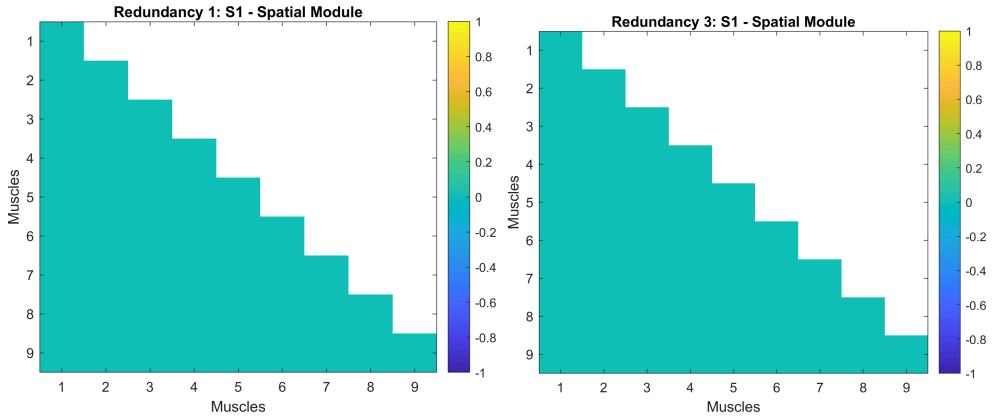

Figure 3.7
Spatial redundancy heatmaps for (A) Participant 1; (B) Participant 3;

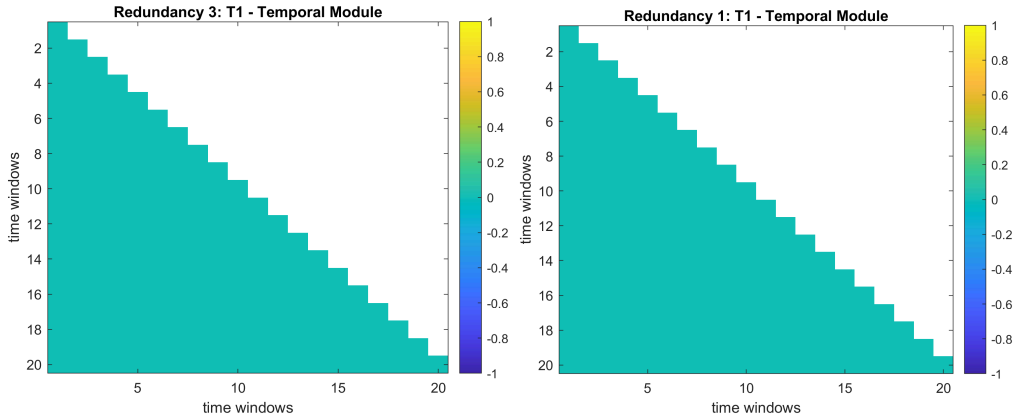

Figure 3.8
Temporal redundancy heatmaps for (A) Participant 1; (B) Participant 3;

3.4 Computation of Mean Spatial and Temporal Synergy Maps

After generating participant-specific synergy heatmaps, the results across participants were averaged by computing mean synergy matrices in both spatial and temporal domains. This averaging represents group-level muscle coordination patterns, with consistent synergistic coupling generalized beyond individual variability.

The mean synergy matrix was computed across the third dimension, resulting in an averaged two-dimensional representation of mean spatial synergy. This matrix represented the central tendency of synergy strength between each muscle pair across all participants, thus providing a generalized spatial map of coordinated muscle activity. The mean matrix was visualized as a heatmap, where warmer colors indicated stronger average synergistic coupling between muscles.

An identical approach was used for the temporal synergy analysis. In this case, the script was implemented on the variable gripMI.ST_S, which represented the temporal synergy modules corresponding to relationships between time windows within each trial. These matrices were then combined into a three-dimensional array and averaged along the participant dimension to produce the mean temporal synergy matrix. The mean temporal synergy heatmap provided the time-dependent coordination of muscle activity during the grip task, showing when in the movement cycle synergistic relationships tended to emerge.

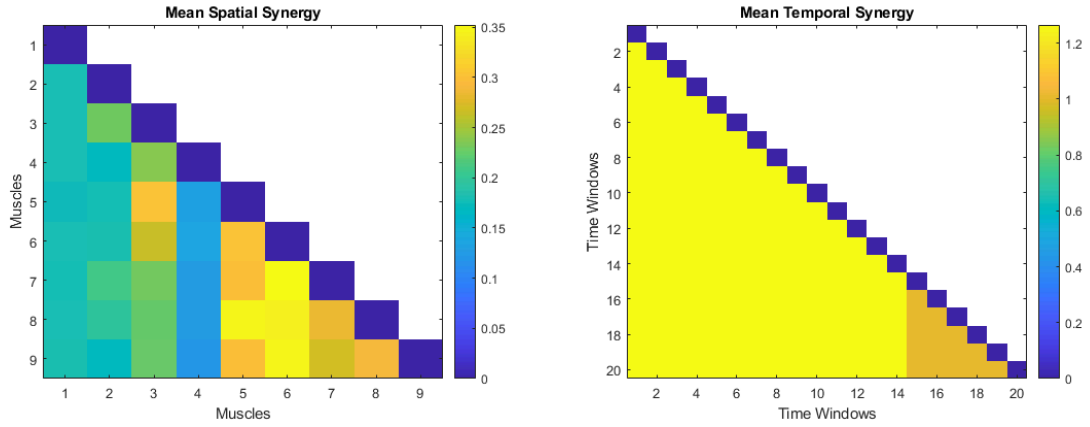

Figure 3.9
Mean synergy heatmaps for all participants (A) Mean spatial synergy; (B) Mean temporal synergy;

3.5 Z-Scoring of Spatial Synergy Maps

To normalize synergy magnitudes across participants and enable group-level statistical comparisons, the spatial synergy matrices were standardized using z-scoring. This normalization step adjusted for interindividual variability in overall synergy strength, allowing a more direct comparison of muscle coordination patterns across the participant group.

Each participant's first synergy component (S1) was selected for analysis, as it typically captured the dominant mode of coordinated muscle activity. For every participant, the script extracted the corresponding vector of pairwise synergy weights. These vectors were then concatenated across all valid participants to form a matrix in which each column corresponded to one participant and each row represented a specific muscle-muscle pair.

The mean and standard deviation of each pairwise synergy value were computed across participants (row-wise). The z-scored synergy values for each participant were then calculated as:

$Z_{ij} = \frac{Xij - \mu i}{\sigma i}$, where X_{ij} is the synergy weight between muscle pair i for participant j, and μ_i and σ_i are the mean and standard deviation of that pair's synergy strength across participants. This transformation expressed each participant's synergy matrix in standard deviation units relative to the group distribution, showing pairs that had unusually strong or weak synergistic coupling compared with the average.

Each participant's z-scored synergy matrix was visualized as a heatmap, where color intensity corresponded to the standardized synergy strength. Warm colors (positive z-values) denoted muscle pairs with stronger-than-average synergistic coordination relative to the group mean, while cool colors (negative z-values) indicated below-average coupling. This normalization made it possible to compare participants on a common scale, independent of individual differences in overall EMG amplitude or synergy magnitude.

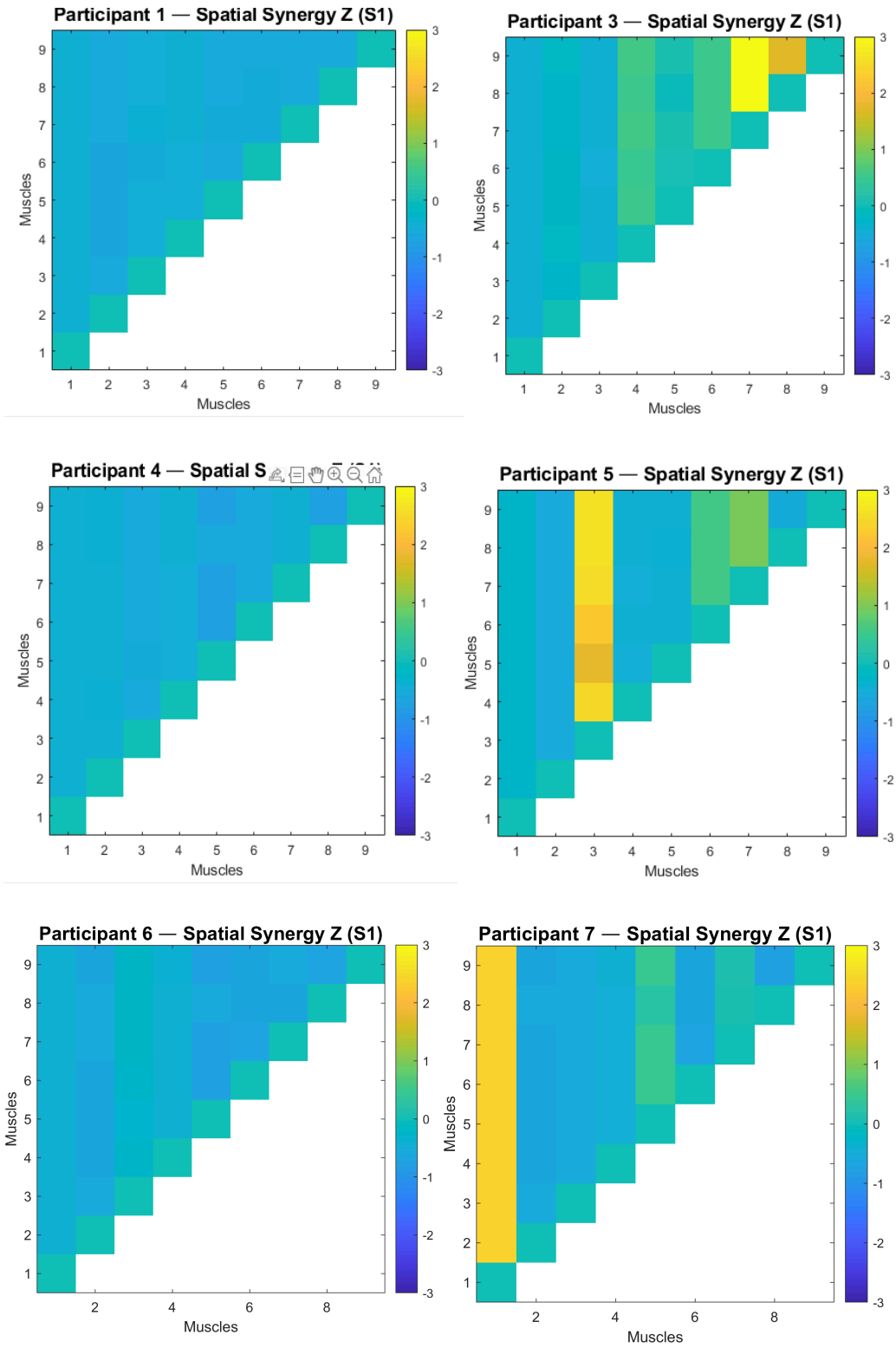

Figure 3.10

Z-scored spatial synergy heatmaps for (A) Participant 1; (B) Participant 3; (C) Participant 4; (D) Participant 5; (E) Participant 6; (F) Participant 7;

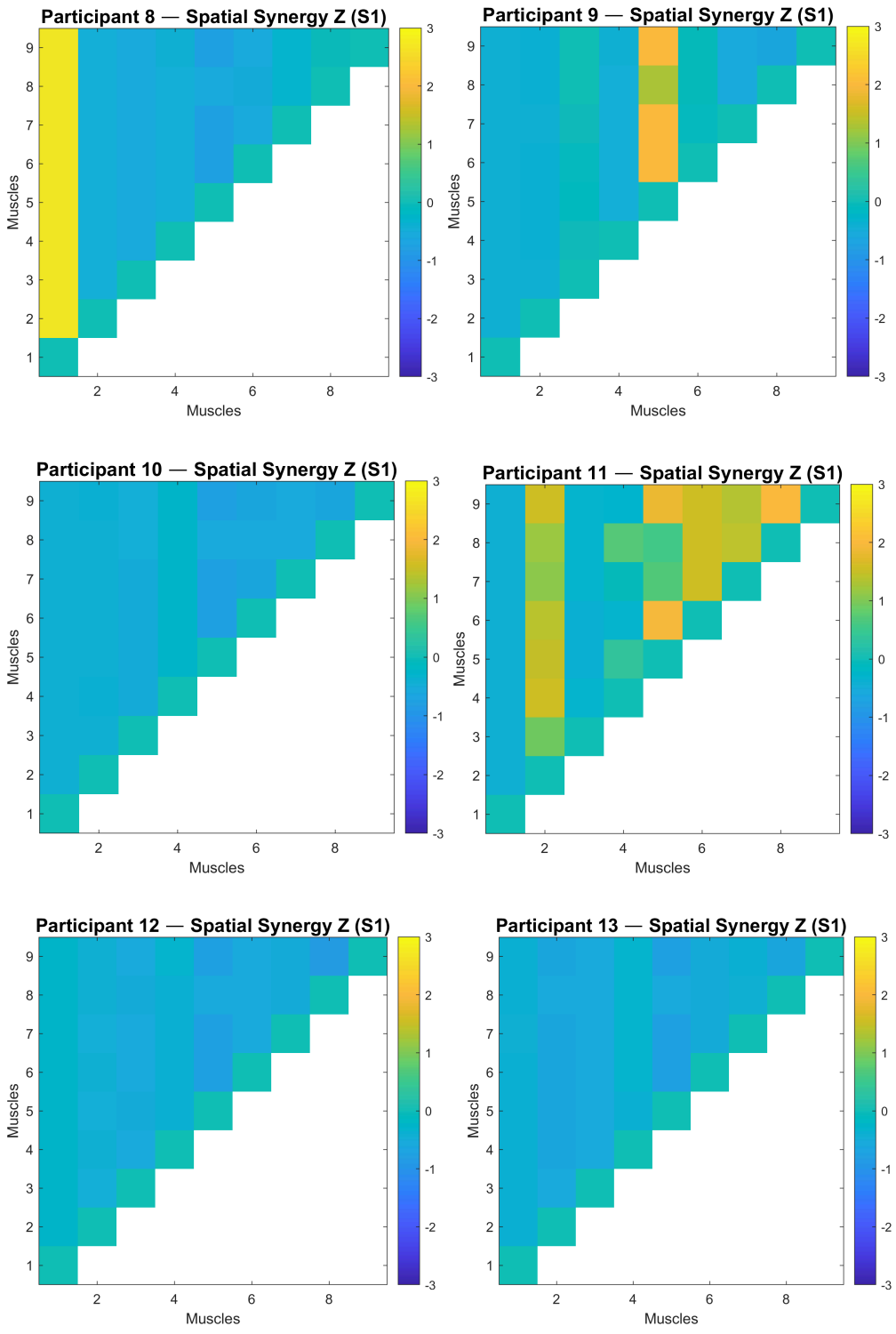

Figure 3.11

Z-scored spatial synergy heatmaps for (A) Participant 8; (B) Participant 9; (C) Participant 10; (D) Participant 11; (E) Participant 12; (F) Participant 13;

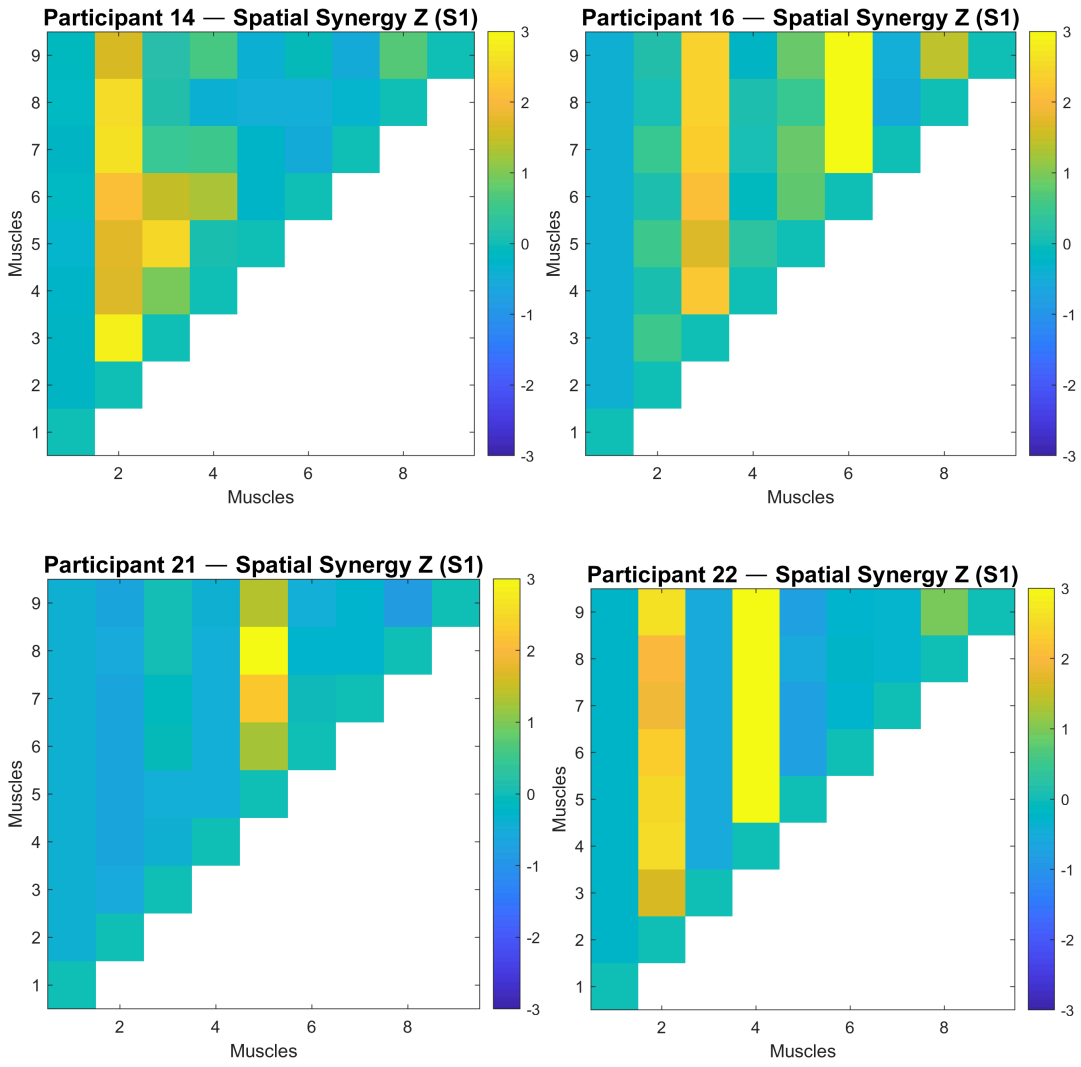

Figure 3.12

Z-scored spatial synergy heatmaps for (A) Participant 14; (B) Participant 16; (C) Participant 21; (D) Participant 22;

3.6 Phase-Amplitude Coupling (PAC) Analysis

To investigate the temporal coordination between low- and high-frequency waves of the muscle signals, Phase-Amplitude Coupling (PAC) analysis was performed on the EMG recordings. PAC quantifies the extent to which the amplitude of higher-frequency oscillations is modulated by the phase of lower-frequency activity. Although PAC is traditionally used in neurophysiological studies involving EEG or MEG to characterize cross-frequency coupling in brain activity, its application to EMG signals offers a means to examine whether similar relationships exist within muscle activation patterns.

In the present analysis, PAC estimation was conducted using the open-source PACmeg toolbox (Seymour, 2020), implemented in MATLAB with the FieldTrip toolbox. The computations followed the method of Tort et al. (2010), which quantifies the degree of phase-amplitude coupling using the *Modulation Index (MI)*. The instantaneous phase of a low-frequency component and the amplitude envelope of a higher-frequency component were extracted via Hilbert transform. The distribution of amplitude values across phase bins was then compared against a uniform distribution using Kullback-Leibler divergence, such that the MI reflected the extent of deviation from uniformity. Higher MI values indicate stronger coupling between the low-frequency phase and the amplitude of the higher-frequency signal, suggesting organized, frequency-specific coordination.

PAC analysis was performed on a subset of participants whose spatial synergy maps displayed visually discernible regions of high synergistic intensity. Participants whose z-scored synergy matrices showed uniformly low or near-zero values across all muscle pairs were excluded from PAC computation.

For the selected participants, a pair of EMG channels corresponding to the muscles that exhibited the strongest synergy were chosen for PAC computation. The first and second channel indices for each participant were defined manually based on the synergy heatmaps and entered into the analysis script as arrays chan_first and chan_second.

The EMG data were drawn from the EMG_accept_Lift structure. Each entry contained multiple trials of rectified EMG activity for individual participants and channels. The EMG data were first rectified using the absolute value, and each trial was interpolated using spline interpolation to a fixed length of 3,500 samples to ensure temporal uniformity across trials. The sampling rate was set to 1,000 Hz. For each selected channel, all valid trials were extracted and processed into a two-dimensional matrix (trials × time). This structure was used as the input for the PAC computation.

For each participant and selected muscle channel, PAC was computed using the following configuration parameters within the PACmeg function:

Sampling frequency (Fs): 1000 Hz
Phase frequency range: 2-8 Hz (1 Hz steps)
Amplitude frequency range: 30-100 Hz (2 Hz steps)
Filter order: 3 (Butterworth, two-pass)
Amplitude bandwidth: ±10 Hz around each amplitude frequency
Method: 'tort' (Modulation Index by *Tort et al., 2010*)
Averaging: PAC values were averaged across all trials

The algorithm first band-pass filtered the EMG signal around each frequency of interest for both the phase and amplitude frequency bands using FieldTrip's bandpass filter. The instantaneous phase of the low-frequency component and the amplitude envelope of the high-frequency component were then extracted via Hilbert transform. The Modulation Index was calculated for every combination of phase and amplitude frequencies, generating a comodulogram matrix where each element represented the MI value for a specific frequency pair.The process was repeated for all selected participants and channels, and the comodulograms were saved in MATLAB figure format.

The resulting PAC matrices were visualized as 2D heatmaps (comodulograms), with the phase frequencies plotted along the horizontal axis and the amplitude frequencies along the vertical axis. The color intensity represented the Modulation Index (MI), reflecting the strength of coupling between low-frequency phase and high-frequency amplitude components.

These PAC comodulograms provide a frequency-domain representation of interdependence between oscillatory components of the EMG signal. Regions of high MI (warm colors) indicate that the amplitude of faster oscillations systematically varies with the phase of slower oscillations, suggesting structured modulation patterns within the muscle signal. Conversely, areas of low MI (cool colors) indicate weak or absent coupling.

Although traditionally interpreted in the context of EEG signal oscillations, in this study, PAC applied to EMG signals can reveal temporal coordination mechanisms in muscle activity. High PAC regions correspond to consistent modulation of high-frequency muscle activation bursts by slower oscillatory processes, potentially reflecting control dynamics or mechanical resonance properties inherent to the motor output.

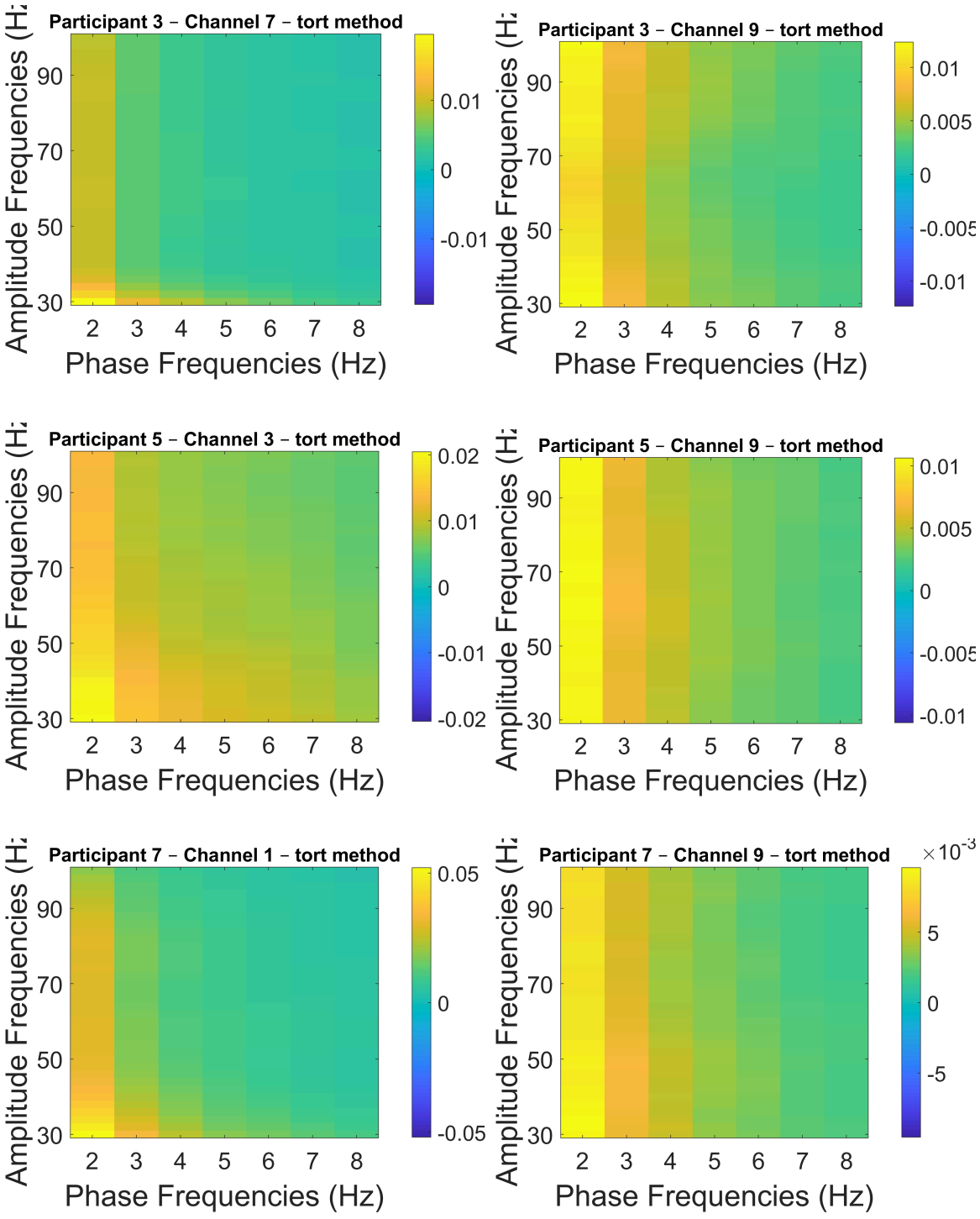

Figure 3.13

Phase-amplitude coupling (PAC) comodulogram for (A) Participant 3-channel 7; (B) Participant 3-channel 9; (C) Participant 5-channel 3; (D) Participant 5-channel 9; (E) Participant 7-channel 1; (F) Participant 7-channel 9;

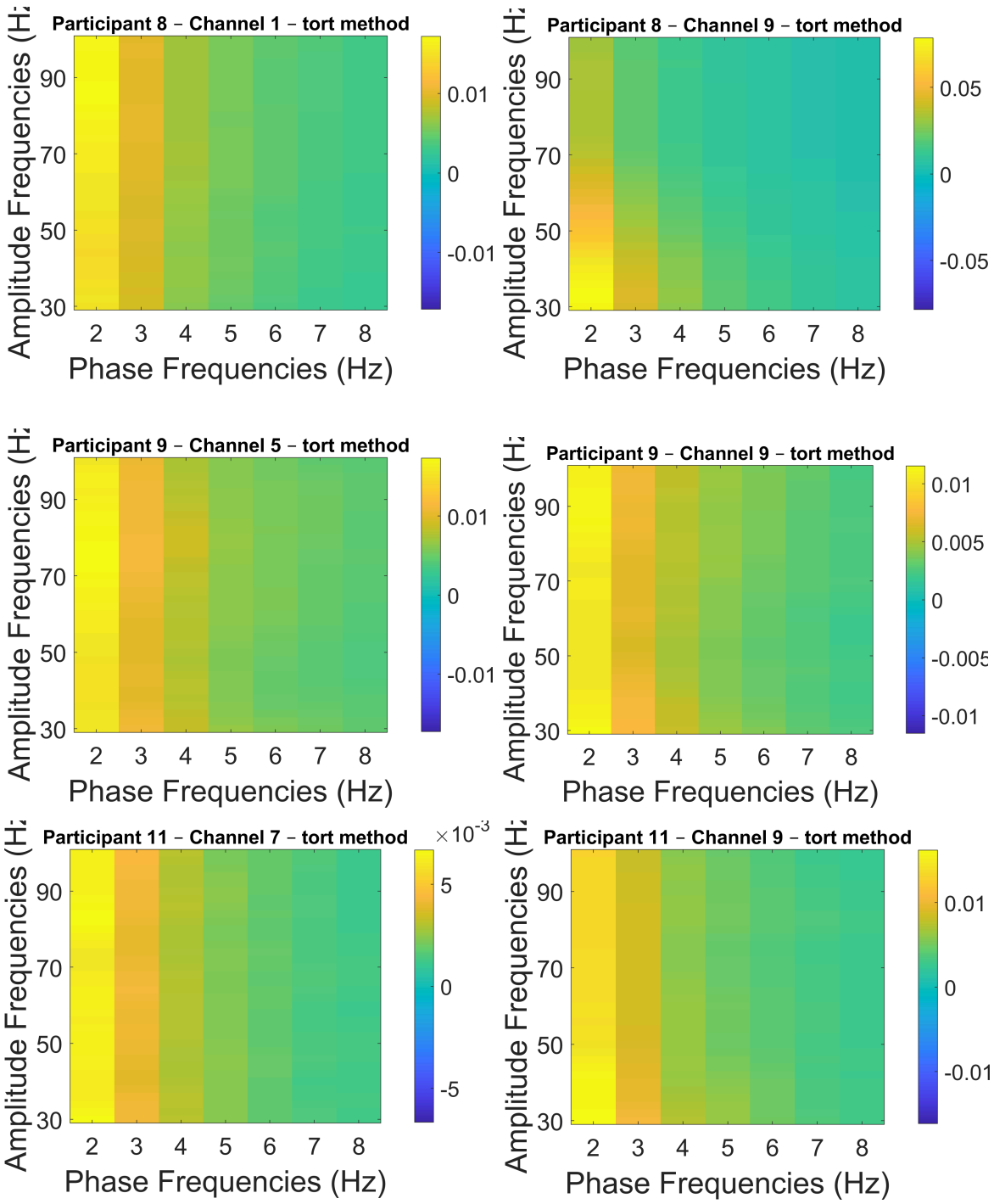

Figure 3.14

Phase-amplitude coupling (PAC) comodulogram for (A) Participant 8-channel 1; (B) Participant 8-channel 9; (C) Participant 9-channel 5; (D) Participant 9-channel 9; (E) Participant 11-channel 7; (F) Participant 11-channel 9;

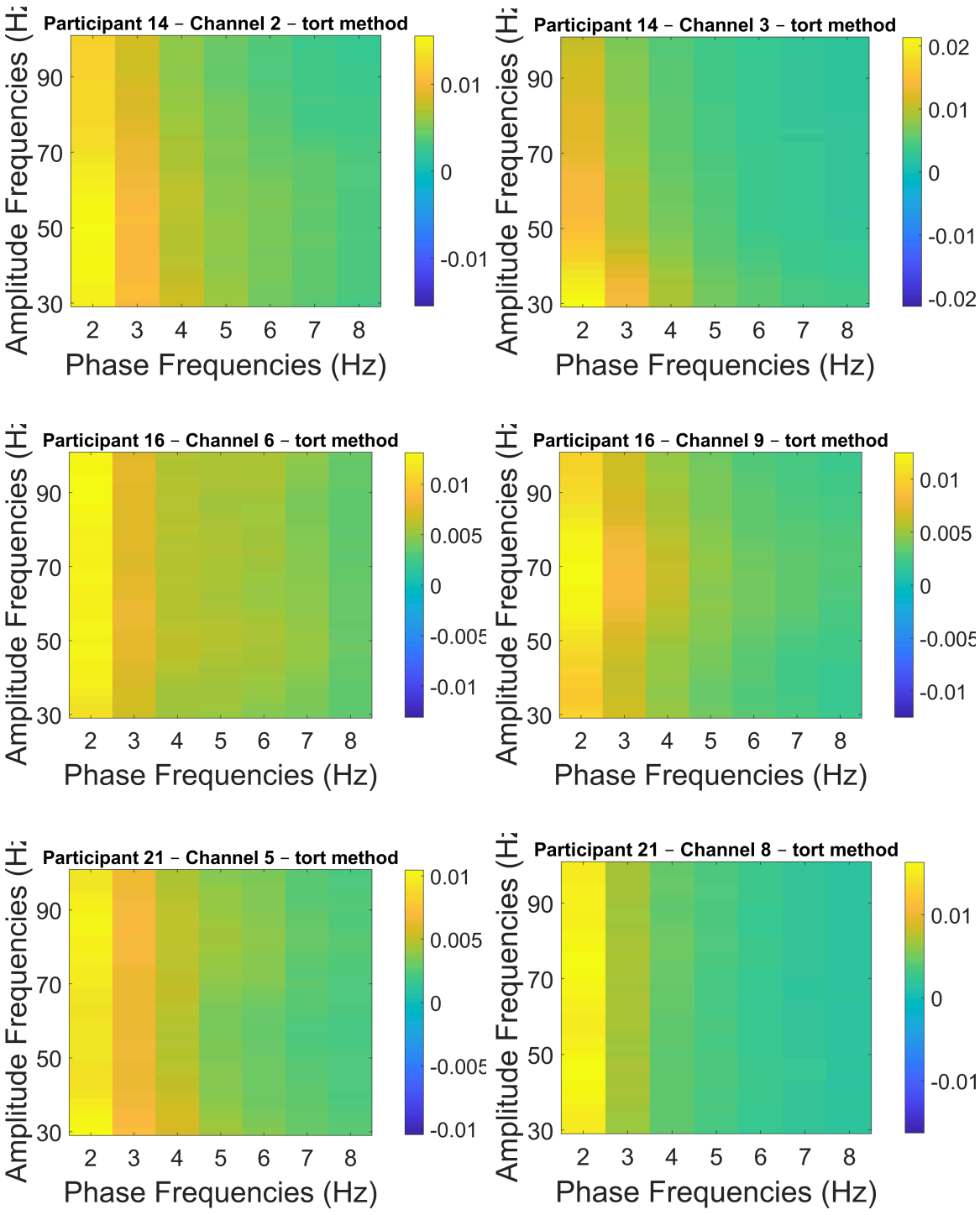

Figure 3.15

Phase-amplitude coupling (PAC) comodulogram for (A) Participant 14-channel 2; (B) Participant 14-channel 3; (C) Participant 16-channel 6; (D) Participant 16-channel 9; (E) Participant 21-channel 8; (F) Participant 21-channel 5;

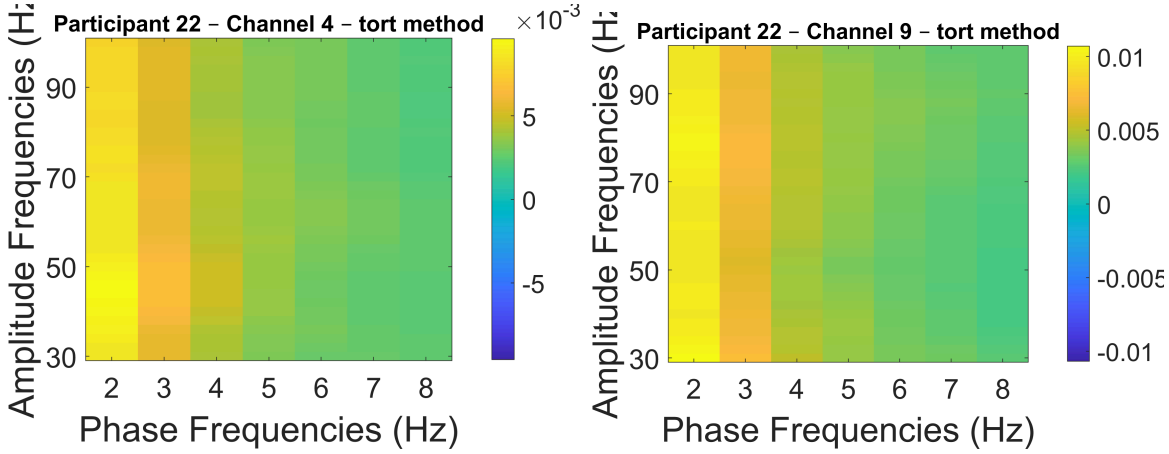

Figure 3.16
Phase-amplitude coupling (PAC) comodulogram for (A) Participant 22-channel 4; (B) Participant 22-channel 9;

3.7 Z-Scoring of Modulation Index (MI) Maps

The individual Modulation Index (MI) matrices obtained from the PAC computations were z-scored separately for each participant and channel. This normalization step allowed direct comparison across participants by removing differences in the absolute scale of PAC values that can arise from signal amplitude variation across participants or recording noise.

This produced a z-scored PAC matrix, representing the relative strength of each phase-amplitude interaction in standard deviation units. Positive z-values indicate frequency pairs with stronger-than-average coupling for that participant and channel, while negative values indicate weaker coupling.

Each z-scored PAC map was visualized using the plot_comod function from the PACmeg toolbox, producing a color-coded heatmap of standardized MI values. Warmer colors represent frequency pairs with coupling strength above the participant's mean, whereas cooler colors indicate below-average coupling. For each participant and channel, the procedure generated a z-scored PAC matrix and a corresponding heatmap figure.

Z-scoring facilitated the subsequent group-averaging analyses by standardizing PAC distributions across individuals, ensuring that differences in absolute PAC magnitude did not bias the comparison of coupling patterns.

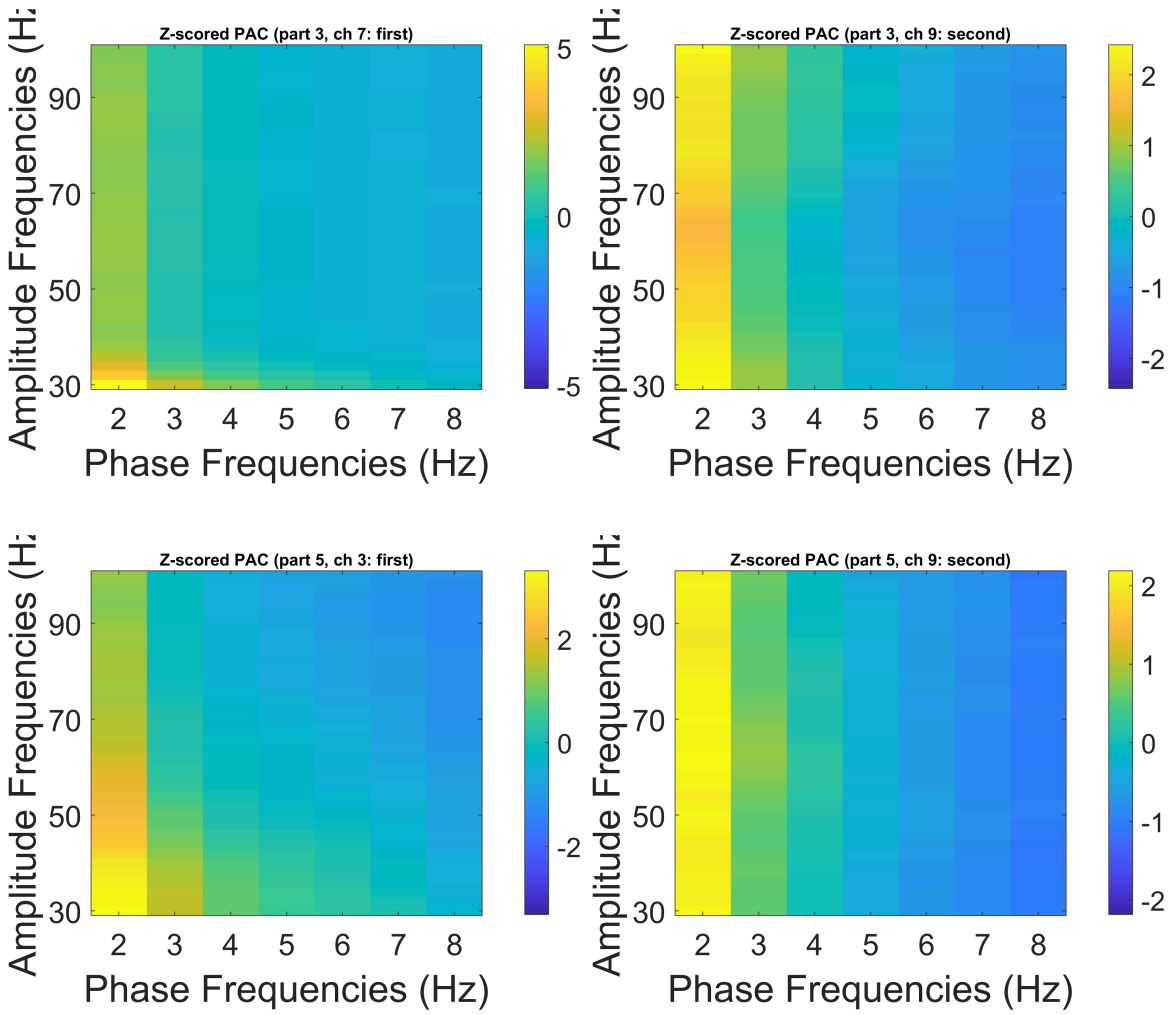

Figure 3.17

Z-scored PAC comodulogram for A) Participant 3-channel 7; (B) Participant 3-channel 9; (C) Participant 5-channel 3; (D) Participant 5-channel 9;

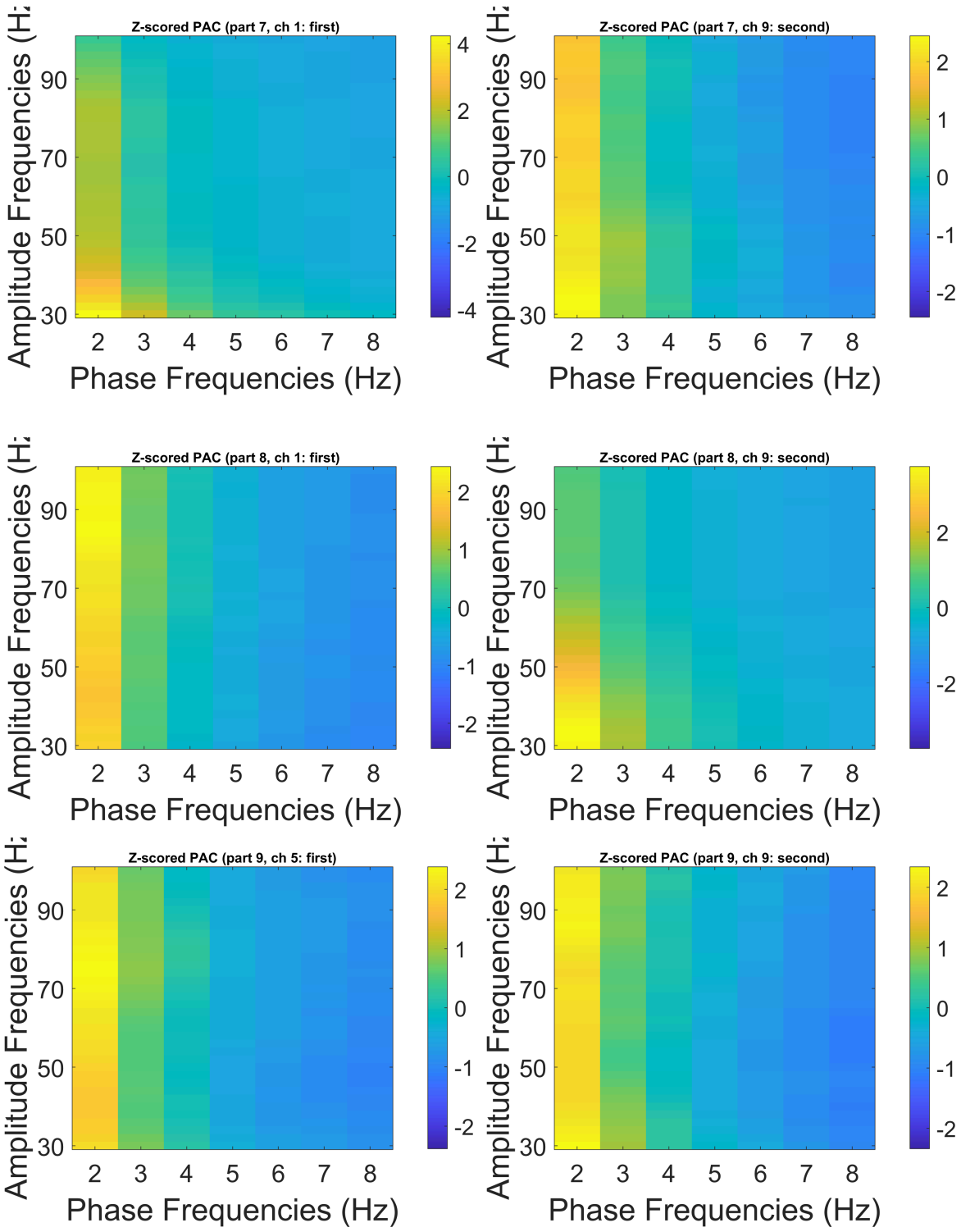

Figure 3.18

Z-scored PAC comodulogram for (A) Participant 7-channel 1; (B) Participant 7-channel 9; (C) Participant 8-channel 1; (D) Participant 8-channel 9; (E) Participant 9-channel 5; (F) Participant 9-channel 9;

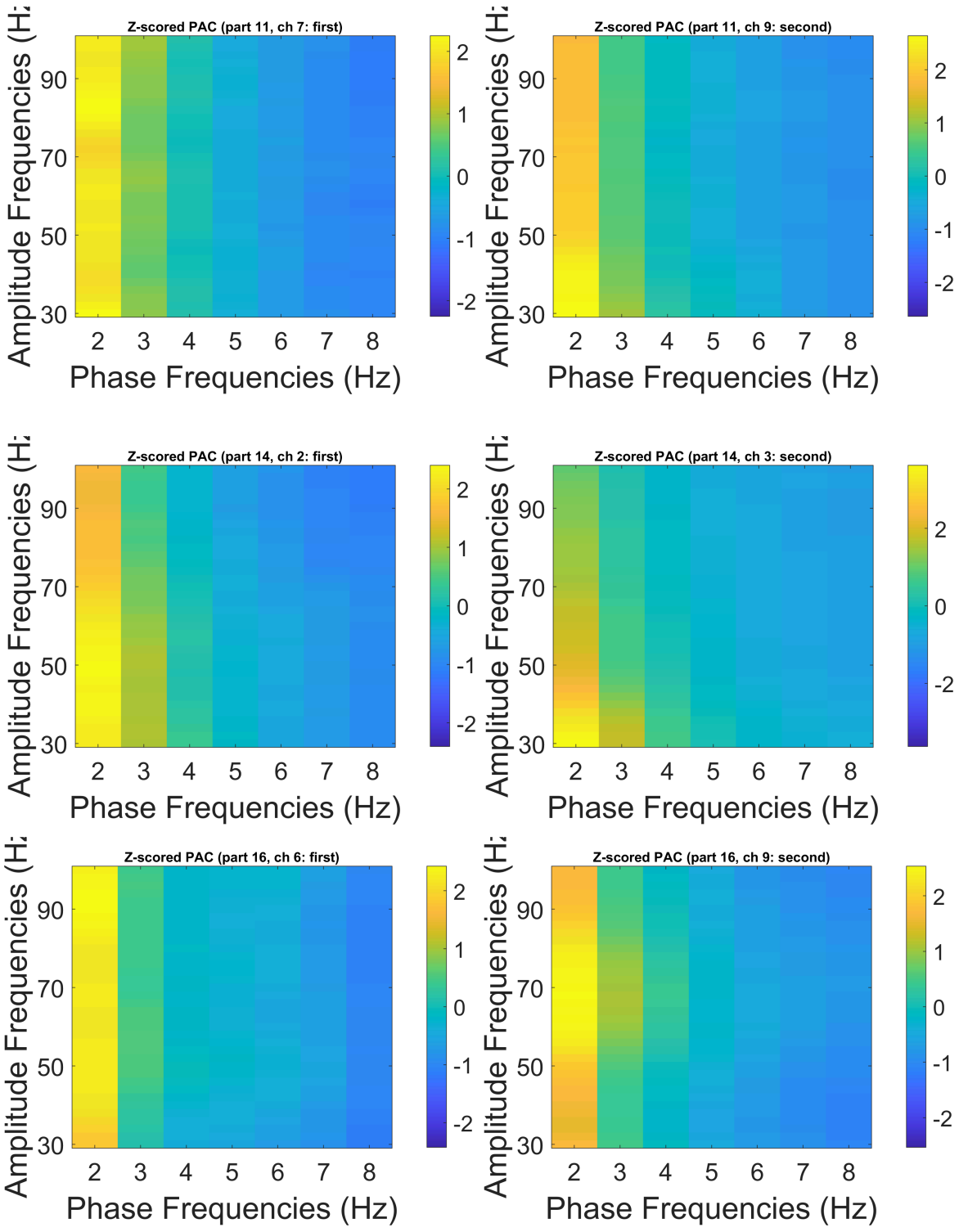

Figure 3.19

Z-scored PAC comodulogram for (A) Participant 11-channel 7; (B) Participant 11-channel 9; (C) Participant 14-channel 2; (D) Participant 14-channel 3; (E) Participant 16-channel 6; (F) Participant 16-channel 9;

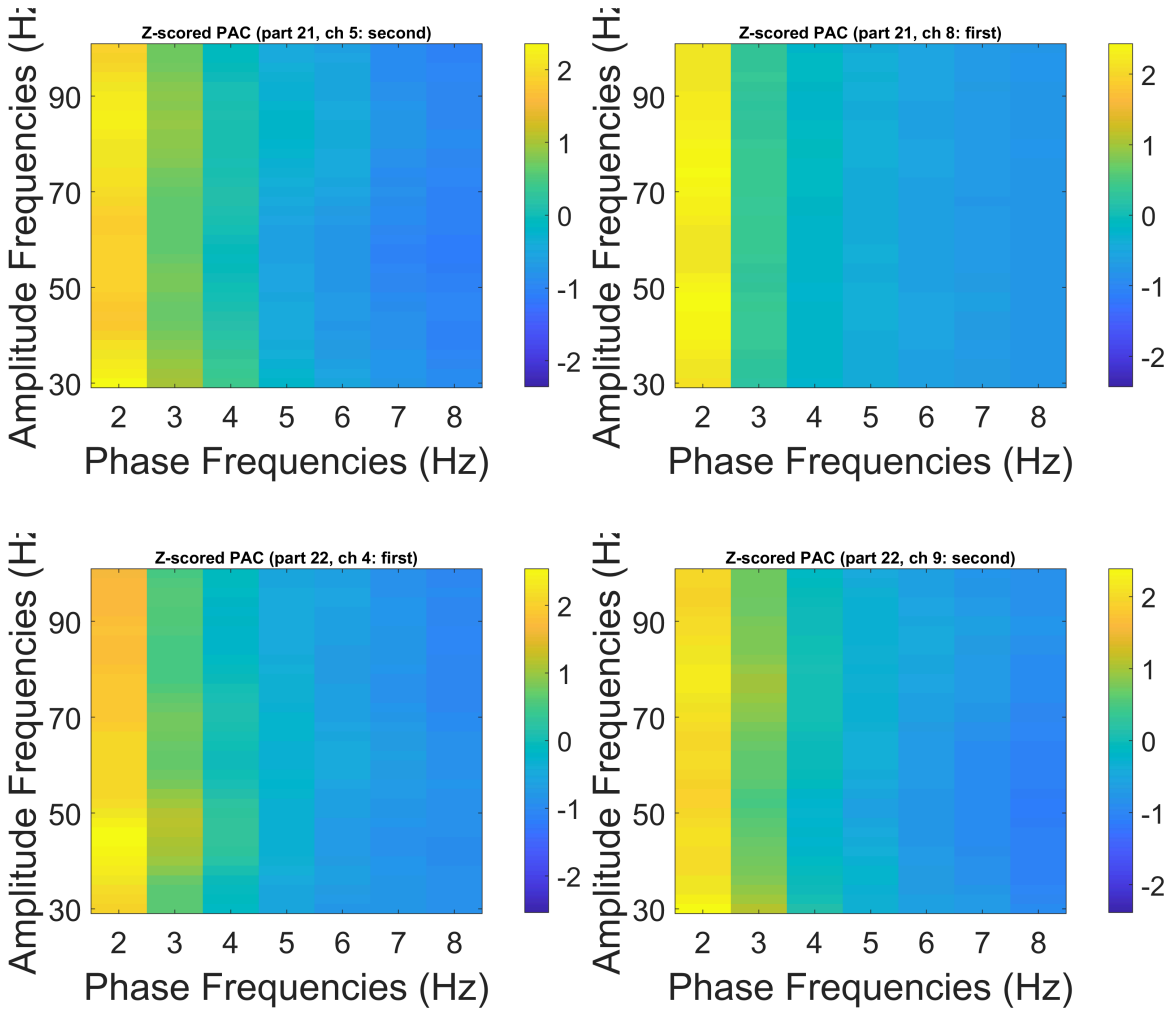

Figure 3.20

Z-scored PAC comodulogram for (A) Participant 21-channel 8; (B) Participant 21-channel 5; (C) Participant 22-channel 4; (D) Participant 22-channel 9;

3.8 Participant and Channel Selection

Only participants who exhibited distinct synergy patterns in their z-scored spatial synergy matrices were included in further PAC analysis. Participants were selected based on the presence of clearly visible regions of high synergy intensity in the heatmaps. Participants whose synergy maps displayed uniformly low z-scored values across all muscle pairs were excluded.

The selection of channels for each participant was based on the observed synergy distribution in the spatial heatmaps. The first channel corresponded to the muscle that demonstrated the highest overall synergy with most other muscles. In the z-scored synergy heatmaps, this typically appeared as a bright yellow vertical column, indicating that this muscle exhibited strong coordinated activity with multiple others. Whenever possible, this muscle was chosen as the first channel.

The second channel was selected as a muscle that also showed high synergy, but with fewer muscle partners. This was represented by a bright yellow square within the yellow column corresponding to the first channel, a locally strong but more selective synergy relationship. This ensured that both globally and locally synergistic muscles were represented in the PAC analysis.

Table 3.1
Participant selection and corresponding muscle channels used for PAC analysis.

Participant	First Channel	Second Channel
3	7	9
5	3	9
7	1	9
8	1	9
9	5	9
11	7	9
14	2	3
16	6	9
21	8	5
22	4	9

3.9 Region-of-Interest (ROI) of PAC Maps

A region-of-interest (ROI) analysis was conducted to obtain quantitative summaries of coupling strength in the most prominent frequency region across participants. This approach focused on the area of the comodulogram that consistently showed the strongest modulation.

The ROI was defined as the 2 Hz phase-frequency column spanning all amplitude frequencies between 30 Hz and 100 Hz. This column represents the coupling between the lowest analyzed phase frequency (2 Hz) and the full range of high-frequency amplitude components.

The choice of this particular phase-frequency column was based on visual inspection of the individual PAC maps. The first column (2 Hz) consistently showed the highest Modulation Index values across participants and channels. The strongest phase-amplitude coupling appeared to occur at this low phase frequency, suggesting that slower rhythmic components of the EMG signal modulated the amplitude of faster muscle activity.

For each participant and for both the first and second selected muscle channels, two data types were analyzed, raw modulation index matrices, and z-scored modulation index matrices. These were standardized versions of the raw matrices, where each MI value was expressed relative to the participant's mean and standard deviation.

For every participant-channel pair, the column corresponding to phase frequency of 2 Hz and amplitude range of 30-100 Hz was extracted. The median MI values were computed for that column, representing the average coupling strength between the 2 Hz phase and all higher amplitude frequencies. The median values were then computed for the z-scored matrices, the resulting values are shown in table 3.2. Higher mean or median values indicate stronger low-frequency modulation of the high frequency oscillations within the EMG signal.

3.10 Selection of Representative Channels Based on Z-Scored PAC Strength

Following the computation and z-scoring of the individual phase-amplitude coupling maps, a selection procedure was performed to identify the representative channel for each participant. This step aimed to determine which muscle channel exhibited the strongest coupling pattern within the region of interest (ROI), allowing subsequent group-level averaging to focus on the most relevant signal for each participant.

The region of interest was defined as the 2 Hz phase-frequency column, corresponding to the lowest analyzed phase frequency, across all amplitude frequencies between 30 and 100 Hz. By focusing on this region, the analysis concentrated on the modulation of high-frequency amplitude components by slow oscillatory activity within the EMG signal.

For each participant and for both of these channels, the z-scored PAC matrices were loaded, and the median values were calculated within the selected region of interest. These values indicate the average and central tendency of standardized PAC strength across the amplitude range for the 2 Hz phase frequency. To identify the representative channel per participant the

channel with the higher median z-scored PAC value within the ROI was selected. If the two channels had identical values, the first channel was retained by default.

Once the representative channel had been identified for each participant, group-level averages were computed. This produced group-average PAC matrices based on channels selected according to the higher ROI median. Each matrix represented the mean of all participants' z-scored Modulation Index values across the full amplitude-phase frequency grid, averaged only from the channels showing the strongest coupling effects. These group averages provided a standardized depiction of PAC strength across participants, allowing consistent visualization of the most dominant low-frequency phase modulation of high-frequency activity.

All computations were implemented in MATLAB. For each participant and channel, the script first loaded the existing z-scored PAC file. The ROI median was calculated from the 2 Hz phase column spanning the 30-100 Hz amplitude rows. The representative channel for each participant was then determined by comparing the ROI metrics between the two available channels. Following selection, the corresponding z-scored PAC matrices were combined to create the group-average maps. The procedure also produced summary tables listing, for each participant, the ROI median values, the selection outcome, and the final representative channel.

The resulting group-average PAC maps were visualized as color-coded comodulograms, showing amplitude frequency on the y-axis and phase frequency on the x-axis. In these figures, warmer colors indicated stronger standardized coupling. The visualizations showed the characteristic structure of low-frequency phase modulation across the population. The use of z-scored data ensured comparability between participants despite differences in overall signal amplitude.

Table 3.2

Median PAC values across participants and channels for the selected ROI, (phase frequency=2 Hz).

Participant	Channel	Median raw	Median z
3	7	0.010	1.875
3	9	0.011	2.107
5	3	0.015	1.569
5	9	0.010	2.087
7	1	0.030	1.819
7	9	0.009	1.994
8	1	0.016	2.091
8	9	0.041	1.425
9	5	0.016	2.097
9	9	0.011	2.036
11	7	0.006	2.039
11	9	0.014	1.991
14	2	0.014	2.077
14	3	0.014	1.755
16	6	0.013	2.227
16	9	0.011	1.979
21	8	0.016	2.275
21	5	0.010	1.984
22	4	0.009	2.067
22	9	0.010	2.037

3.11 Group-Level Averaging of Phase-Amplitude Coupling (PAC)

Following individual PAC computations, a group-level analysis was performed to obtain average PAC maps across participants. This step aimed to measure common cross-frequency coupling patterns and identify frequency ranges that consistently exhibited phase-amplitude modulation across the dataset.

3.11.1 Averaging Procedure

Three separate group averages were computed. The first channel average represents the mean PAC across all first-channel muscles.The second channel average represents the mean PAC across all second-channel muscles. The representative channel average for each participant was the channel, first or second, that exhibited the stronger overall PAC when averaged across all frequency pairs.

The resulting group-average PAC matrices for each condition (first, second, and representative channels) were used to generate heatmaps, using the plot_comod function from the PACmeg toolbox (Seymour, 2020). Each heatmap displayed the phase frequencies (2-8 Hz) on the x-axis and amplitude frequencies (30-100 Hz) on the y-axis. The color intensity indicated stronger phase-amplitude coupling with warmer colors.

Finally, to compute the grand-average PAC, the individual PAC comodulograms from each participant's selected channels were selected, for a total of 20 PAC maps across the 10 participants.

3.11.2 Interpretation

The first-channel group average represents the PAC structure of muscles acting as central coordinators within the synergy network-those that exhibited widespread coupling with other muscles. The second-channel average represents more selective muscles that contributed to localized coordination. The representative-channel average serves as an overall measure of PAC strength by including, for each participant, the channel demonstrating the strongest individual coupling.

These PAC averages provide insights into the hierarchical organization of muscle activation patterns. The maps illustrate frequency regions where high-frequency muscle activity was modulated by the phase of slower oscillatory components, suggesting structured temporal coordination within the EMG signals. More detailed statistical comparisons and interpretations of these PAC patterns are presented in the subsequent Results section.

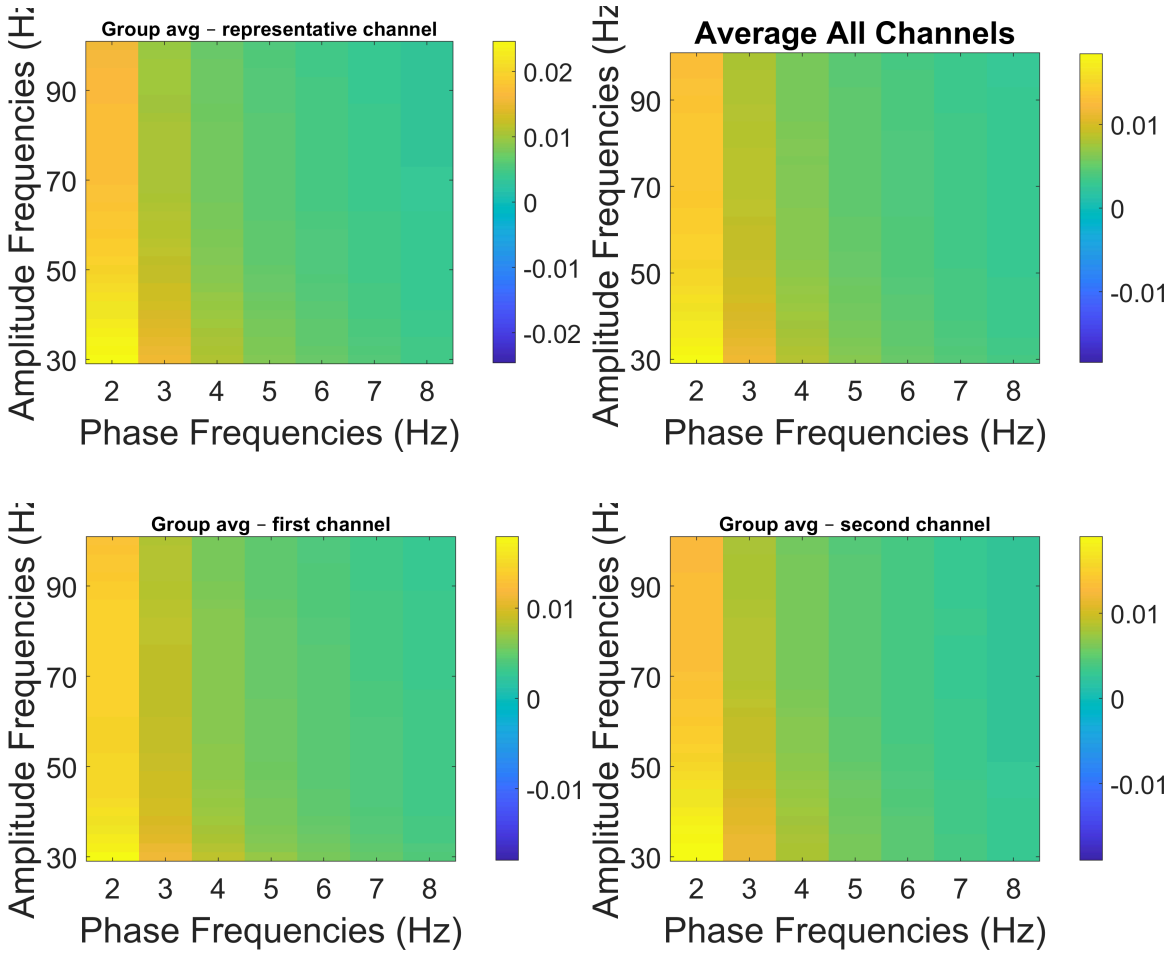

Figure 3.21

Average phase-amplitude coupling comodulogram for (A) representative channels; (B) all channels; (C) first channel chosen; (D) second channel chosen;

3.12 Composite Channel Phase-Amplitude Coupling Analysis

A composite-channel approach was implemented to examine whether the phase-amplitude coupling patterns observed within individual muscles were also present at the level of synergistic muscle pairs. For each participant, the two EMG channels previously identified as functionally related were combined to form a single composite signal. This was achieved by averaging their z-scored activity on a trial-by-trial basis, ensuring that both channels contributed equally regardless of differences in absolute amplitude (Bizzi et al., 2008; Ting and McKay, 2007).

Each EMG trial was first rectified, interpolated to a fixed length of 3,500 samples, and normalized (z-scored) within channel to remove amplitude biases. The two normalized channel signals were then averaged to create the composite waveform, representing the synchronized muscle activity for that trial. This process was repeated across all valid trials for each participant, producing a composite EMG signal.

The resulting composite signals were analyzed using the same PAC configuration parameters applied in the single-channel analyses, employing the Tort et al. (2010) modulation index method to compute coupling between low phase frequency (2-8 Hz) and high amplitude frequency (30-100 Hz). The comodulograms were visualized as color-coded heatmaps, where warmer colors indicated stronger coupling between phase and amplitude frequencies.

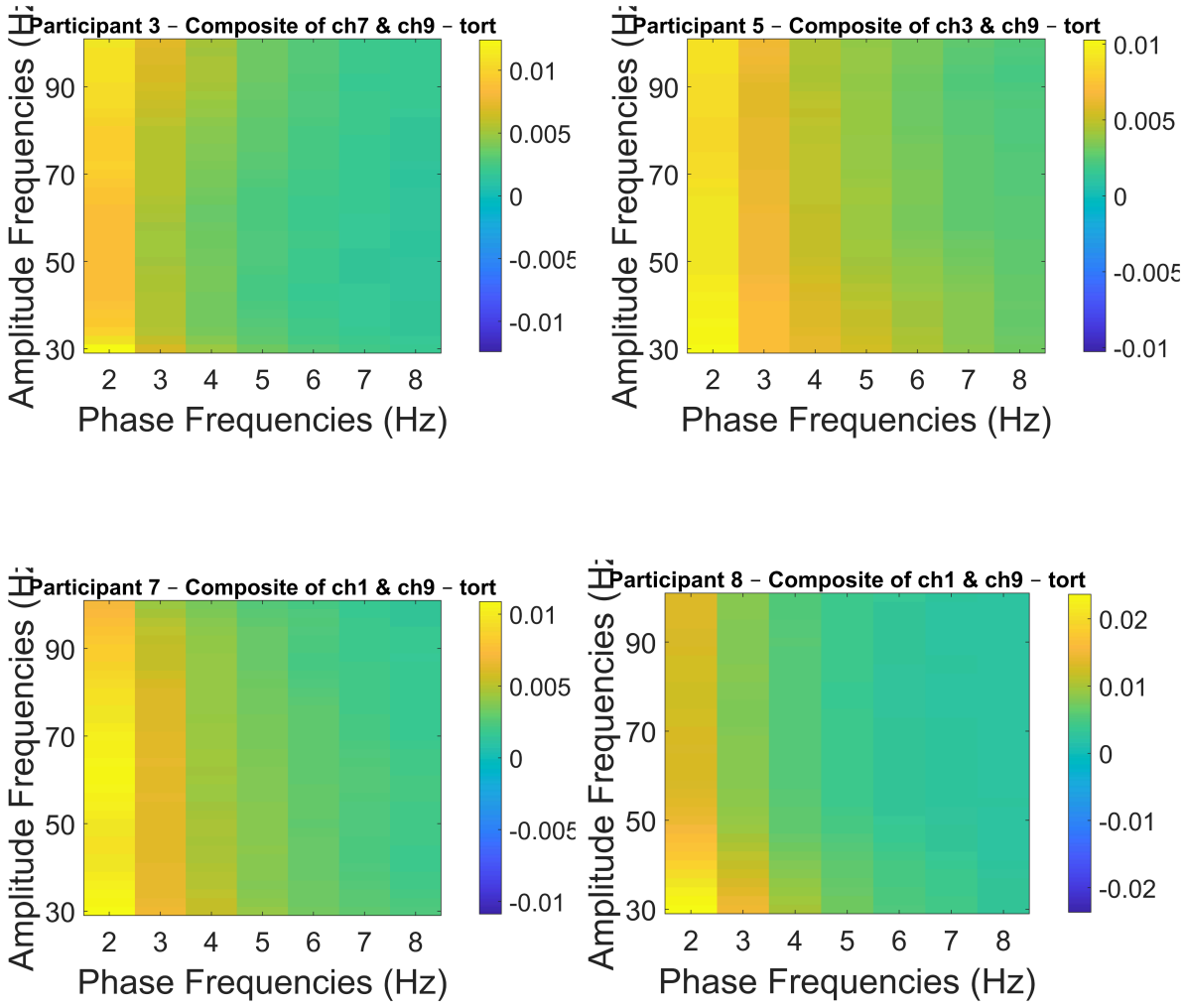

Figure 3.22

Composite PAC comodulogram for (A) Participant 3-channels 7,9; (B) Participant 5-channels 3,9; (C) Participant 7-channels 1,9; (D) Participant 8-channel 1,9;

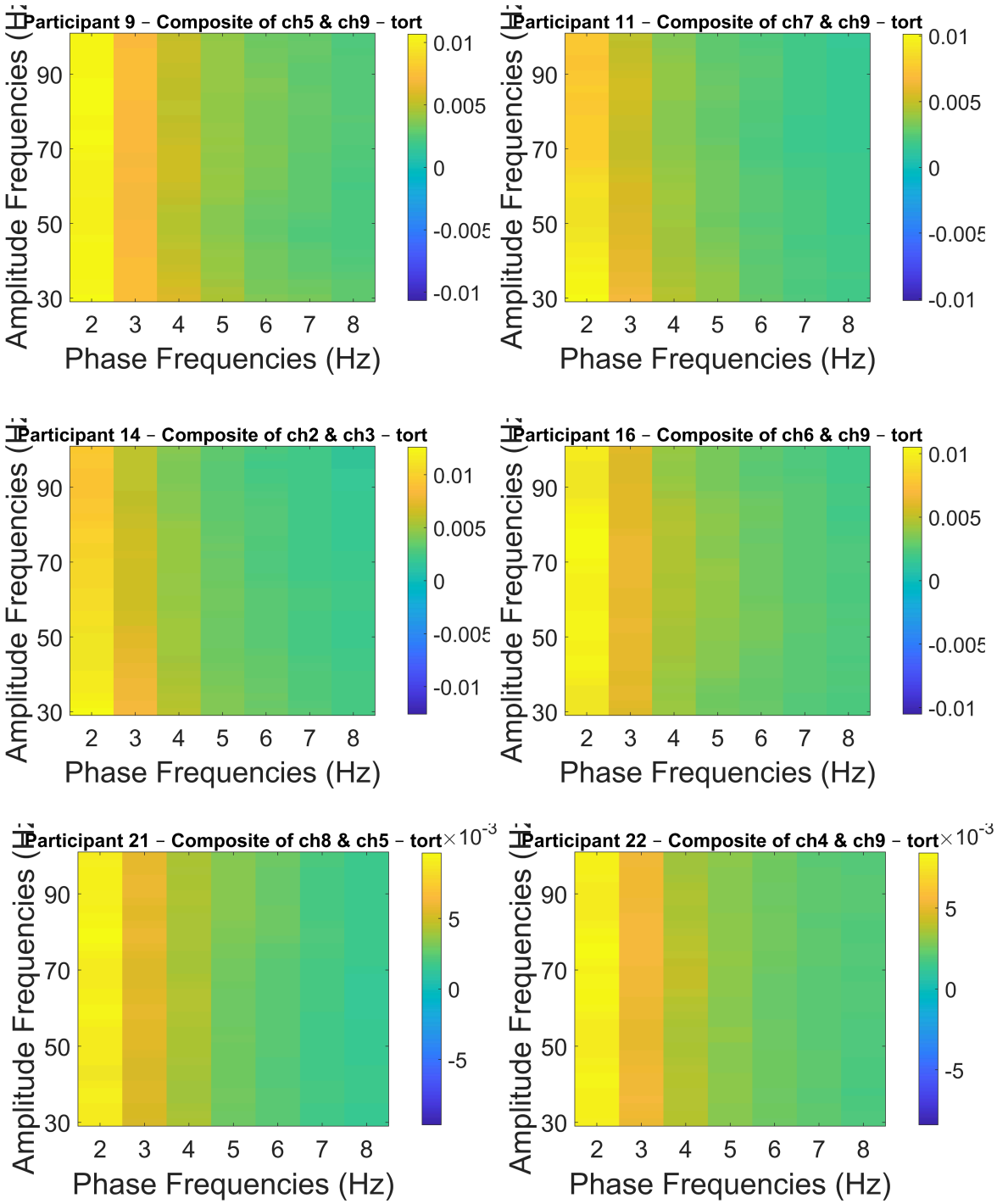

Figure 3.22

Composite PAC comodulogram for (A) Participant 9-channels 5,9; (B) Participant 11-channel 7,9; (C) Participant 14-channel 2,3; (D) Participant 16-channel 6,9; (E) Participant 21-channel 8,5; (F) Participant 22-channel 4,9;

Although few studies have explicitly examined composite or “multi-muscle” PAC in peripheral recordings, related concepts have been explored in EEG and MEG research through joint or multi-site PAC analyses (Canolty et al., 2006; Florin and Baillet, 2015), where coupling is studied across averaged or principal-component signals representing distributed neural sources. The concept of intermuscular coherence has long been used to describe common oscillatory inputs across muscles. The current approach is an exploratory analysis examining whether the phase-amplitude coupling observed within individual muscles persists when synergistically coactive muscles are combined into a composite signal.

A group-average PAC representation was generated from the previously computed composite-channel PAC matrices. Each composite matrix represented the coupling between low-frequency phase and high-frequency amplitude components derived from the averaged EMG signals of two synergistic muscles per participant. To obtain a standardized measure of coupling strength across participants, a region of interest (ROI) was defined as the 2 Hz phase-frequency column spanning the full amplitude range of 30-100 Hz.

For each participant, the median modulation index within this ROI was calculated from the composite PAC matrix, summarizing the coupling strength in the dominant phase-amplitude range. This measure provides an estimate of the participant’s PAC magnitude that was less sensitive to outlier values than the mean. The script then combined all individual composite PAC matrices into a three-dimensional array and computed their mean across participants to obtain a group-average PAC map.

The resulting group-average composite PAC matrix was saved alongside a summary table containing each participant’s ROI median values and corresponding channels. The results were visualized as color-coded comodulograms, where amplitude frequency was plotted on the y-axis and phase frequency on the x-axis, with color intensity representing the strength of coupling. This procedure provided a population-level overview of shared phase-amplitude coupling dynamics between synergistic muscle pairs, emphasizing consistent modulation patterns across participants.

Table 3.3

Median composite PAC values across participants and channels for the selected ROI, (phase frequency=2 Hz).

Participant	First Channel	Second Channel	Composite PAC Median
3	7	9	0.010
5	3	9	0.009
7	1	9	0.010
8	1	9	0.013
9	5	9	0.010
11	7	9	0.008
14	2	3	0.010
16	6	9	0.010
21	8	5	0.009
22	4	9	0.008

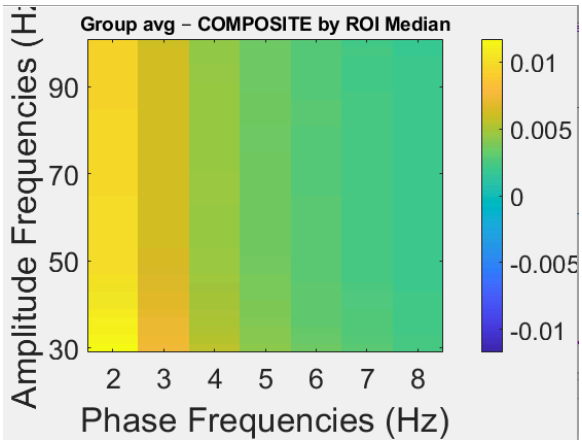

Figure 3.23

Average Composite PAC comodulogram

3.13 Phase-Amplitude Coupling Analysis of EMG Activity With Surrogates

EMG data during the grip force task was analyzed to quantify cross-frequency phase-amplitude coupling using a GPU-accelerated implementation of the Tort Modulation Index. The analysis was performed in Python (Google Colab environment) using NumPy, SciPy, Matplotlib, and PyTorch libraries. All computations were executed on an NVIDIA GPU when available to reduce processing time.

Preprocessed EMG recordings were used, containing trial-wise signals for multiple participants and channels. The recordings from 10 participants, with two selected EMG channels per participant were utilised. Sampling frequency was 1000 Hz, and each trial was temporally normalized to 3500 samples to allow inter-trial comparison.

Each trial underwent rectification (absolute value) and cubic-spline interpolation to a uniform 3500-point temporal grid. For single-channel analyses, the rectified and interpolated signals were used directly, replicating the preprocessing steps of the original MATLAB PACmeg implementation. For composite-channel analyses, each channel was additionally z-scored on a per-trial basis before averaging (composite = 0.5 × [z-score(channel 1) + z-score(channel 2)]), to replicate the MATLAB composite-PAC procedure. The z-scoring step removes amplitude bias between channels and standardizes within-trial variance.

3.14 Time-frequency decomposition using Morlet wavelets

Instantaneous phase and amplitude were derived via convolution with complex Morlet wavelets, implemented in the frequency domain for efficiency. Each wavelet was defined by a Gaussian frequency response centered at a target frequency f_0 with a spectral standard deviation $\sigma_f = f_0 / n_c$, where n_c is the number of wavelet cycles. Phase-carrying (low-frequency) components were extracted at 2-8 Hz using 3 cycles per wavelet, and amplitude-carrying (high-frequency) components were extracted at 30-100 Hz using 6 cycles per wavelet. Fast Fourier transforms were used to perform the convolution across all trials and frequencies.

The analytic wavelet output yields a complex-valued representation for each frequency band and trial. The instantaneous phase was computed as the argument (angle) of the complex signal, and the amplitude envelope was computed as its modulus (absolute value).

3.14.1 Computation of phase-amplitude coupling

PAC strength was quantified using the Tort Modulation Index (MI). For each phase frequency f_p and amplitude frequency f_a, the instantaneous amplitude values were binned according to the phase angle (18 bins from −π to π). The mean amplitude per bin was normalized to form a probability distribution $P(f_a,f_p,\phi)$ over phase angles. Deviation from a uniform distribution was quantified via the Kullback-Leibler divergence:

$$\mathrm{MI}(f_a, f_p) = \frac{1}{\log(N)} \sum_{\phi} P(\phi) \log \frac{P(\phi)}{U}$$

where N is the number of phase bins and U=1/N. The resulting MI values form a two-dimensional comodulogram representing PAC intensity across amplitude-and phase-frequency pairs. All computations were vectorized and performed in PyTorch tensors.

3.14.2 Surrogate-based normalization

A surrogate procedure, with the swap-trial method, was implemented to assess statistical significance. In this approach, amplitude and phase signals from different trials were randomly permuted to generate surrogate MI distributions (200 iterations). The observed MI was then z-scored relative to the surrogate mean and standard deviation, producing a normalized PAC z-score map. This step isolated coupling beyond chance alignment of amplitude bursts and low-frequency phase. For each participant and channel, color-coded PAC heatmaps were generated. The x-axis corresponds to phase frequency, the y-axis to amplitude frequency, and color encodes either raw MI or z-scored MI, depending on analysis type.

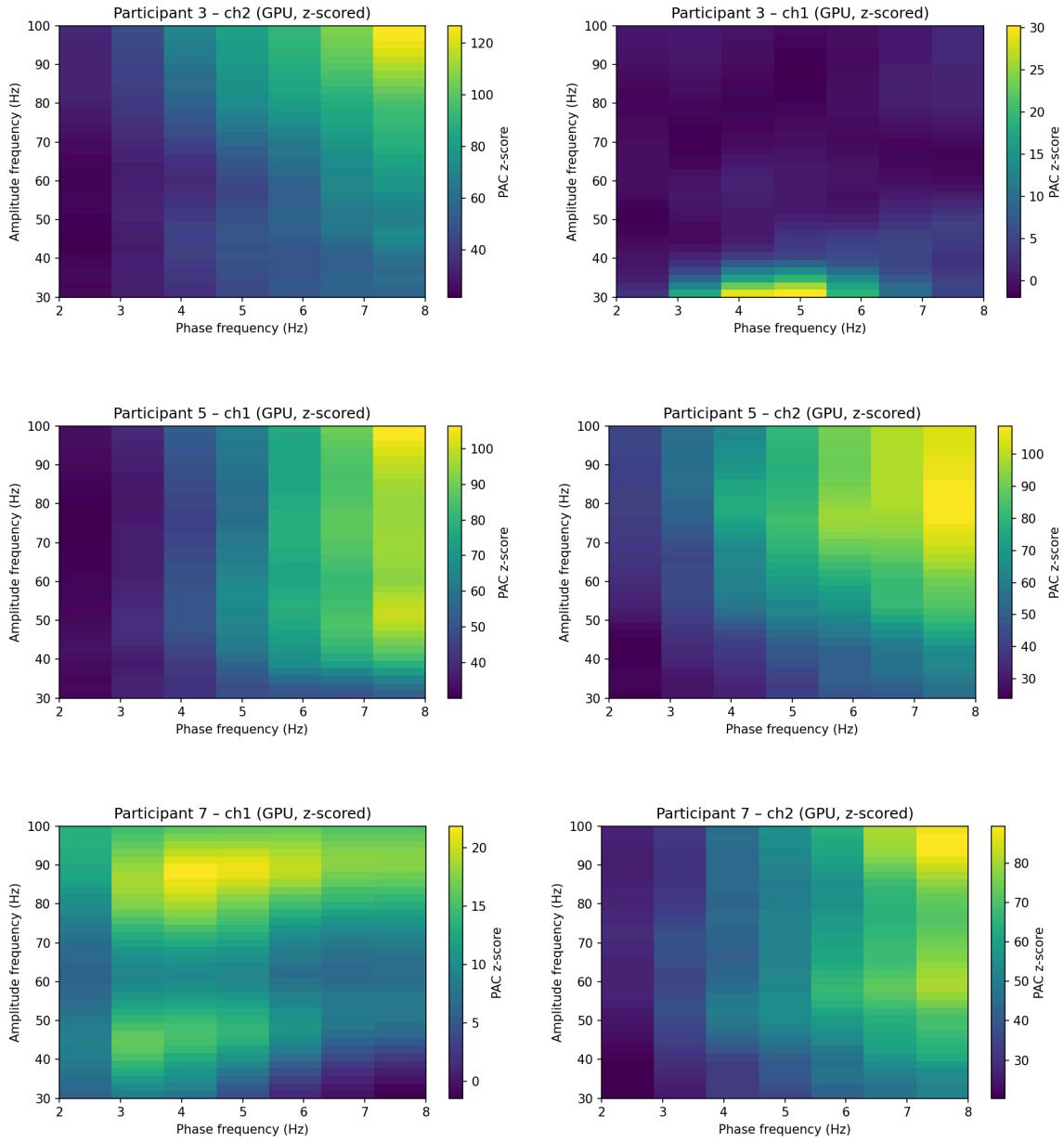

Figure 3.24

Z-scored phase-amplitude coupling (PAC) comodulograms computed using Morlet wavelet convolution and normalized using trial-shuffled surrogates. Results are shown separately for EMG channel 1 (Ch1), channel 2 (Ch2)

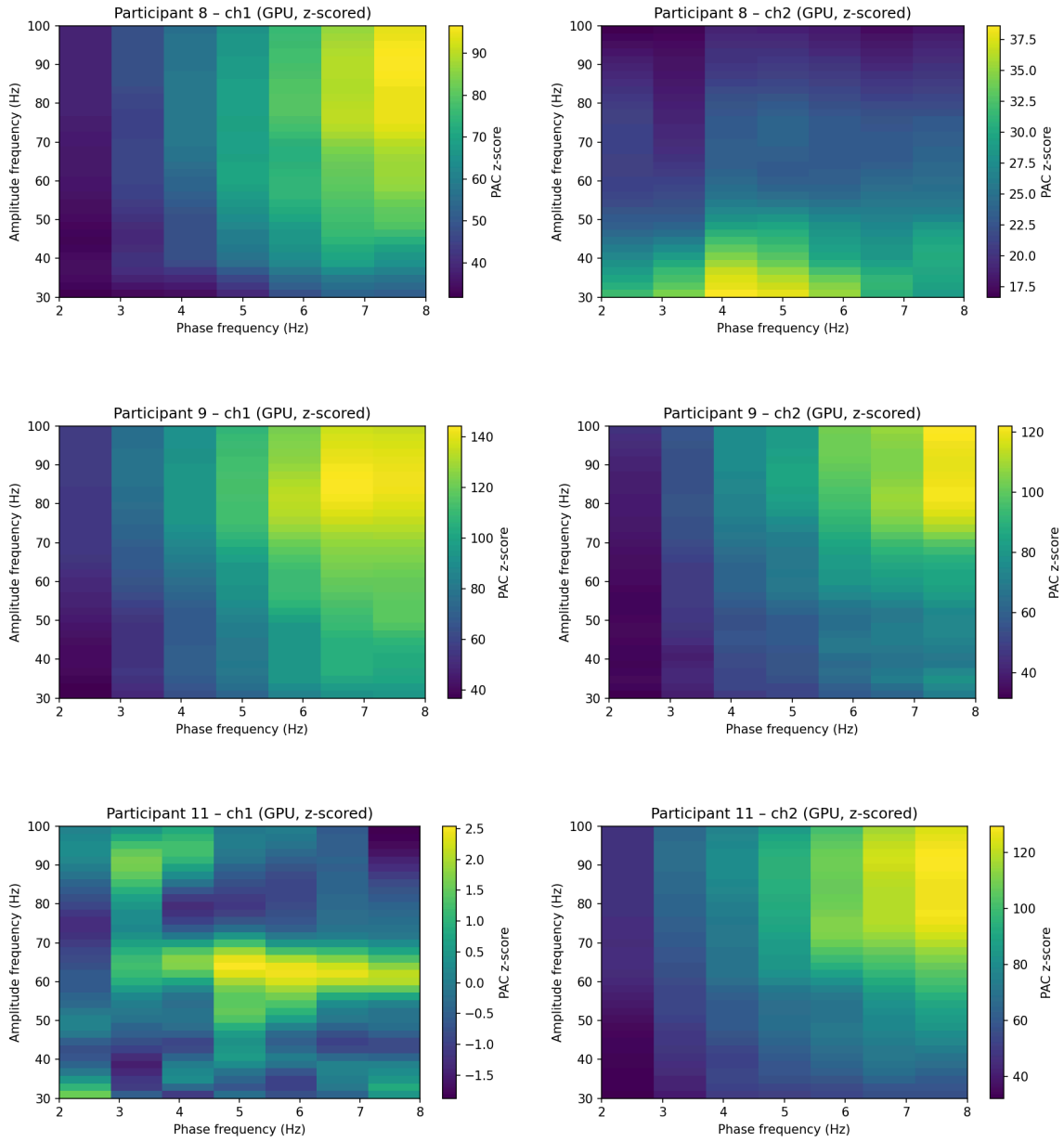

Figure 3.25

Z-scored phase-amplitude coupling (PAC) comodulograms computed using Morlet wavelet convolution and normalized using trial-shuffled surrogates. Results are shown separately for EMG channel 1 (Ch1), channel 2 (Ch2)

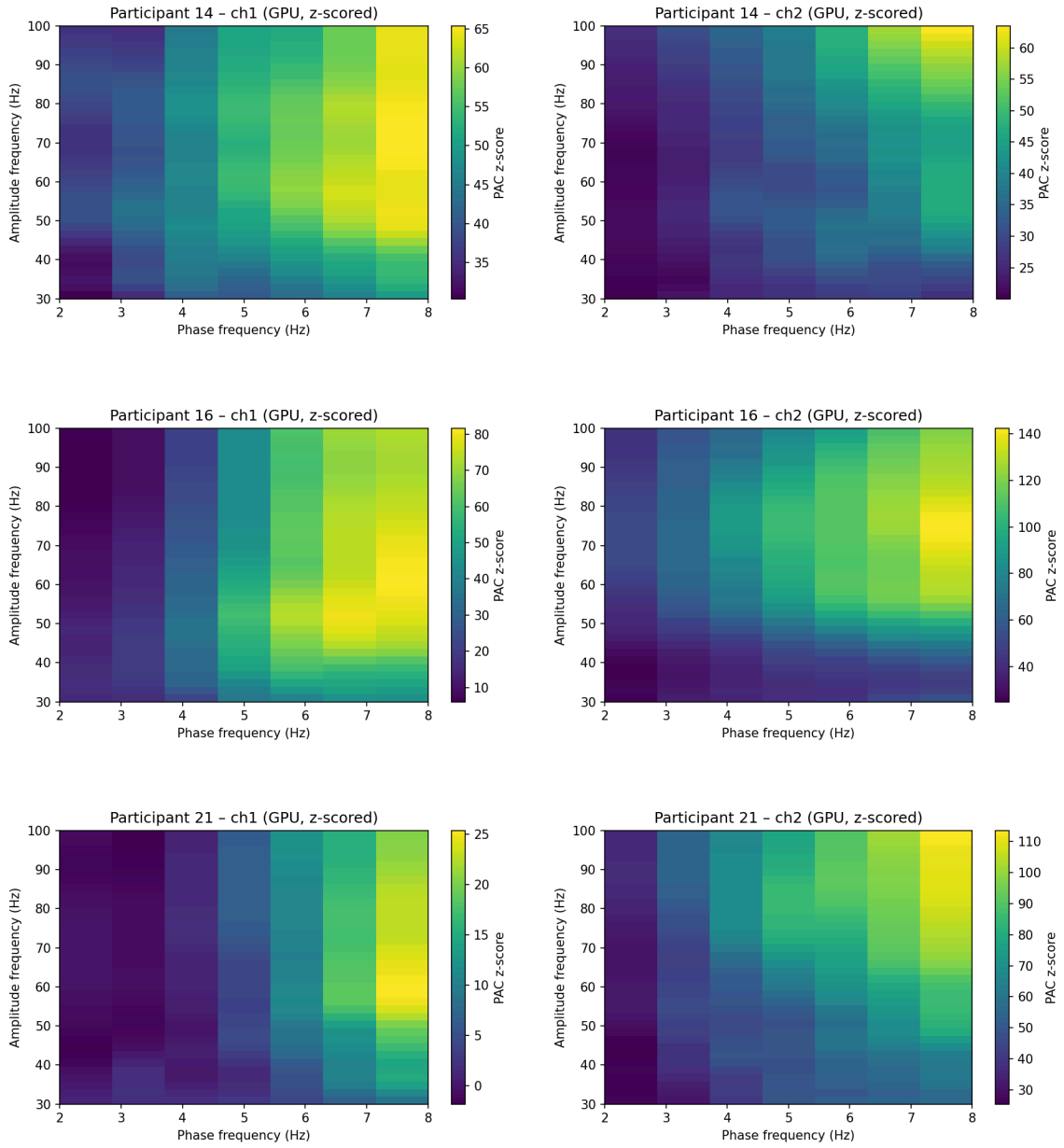

Figure 3.26

Z-scored phase-amplitude coupling (PAC) comodulograms computed using Morlet wavelet convolution and normalized using trial-shuffled surrogates. Results are shown separately for EMG channel 1 (Ch1), channel 2 (Ch2)

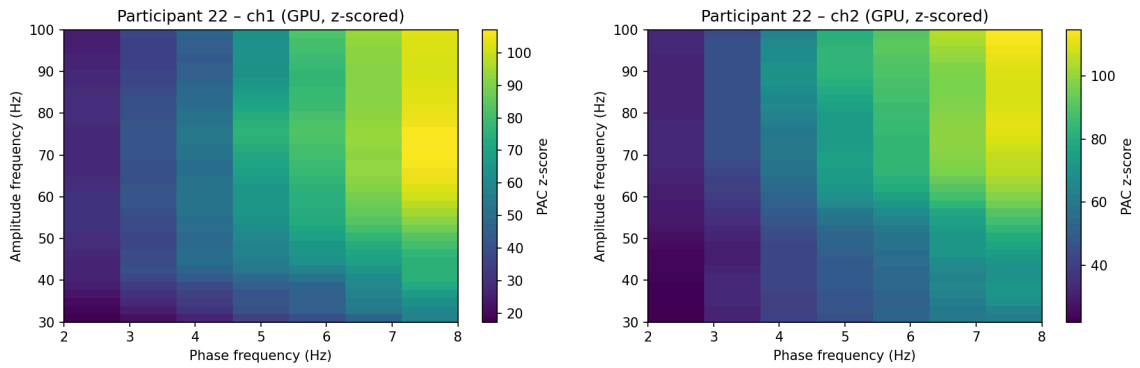

Figure 3.27
Z-scored phase-amplitude coupling (PAC) comodulograms computed using Morlet wavelet convolution and normalized using trial-shuffled surrogates. Results are shown separately for EMG channel 1 (Ch1), channel 2 (Ch2)

Figures 3.24 - 3.27 show the strength of PAC between low-frequency phase (x-axis, 2-8 Hz) and high-frequency amplitude (y-axis, 30-100 Hz) of EMG activity, in each panel. The signals were obtained via complex Morlet wavelet convolution, providing time-frequency-resolved phase and amplitude estimates. PAC was quantified using the Tort Modulation Index, normalized against 200 trial-shuffled surrogates, and expressed as z-scores.

These wavelet-based results contrast with the MATLAB PAC analysis, where Hilbert-transform based phase and amplitude signals were used. Differences between the two methods reflect distinct time-frequency tradeoffs in how the analytic representations capture phase-amplitude relationships.

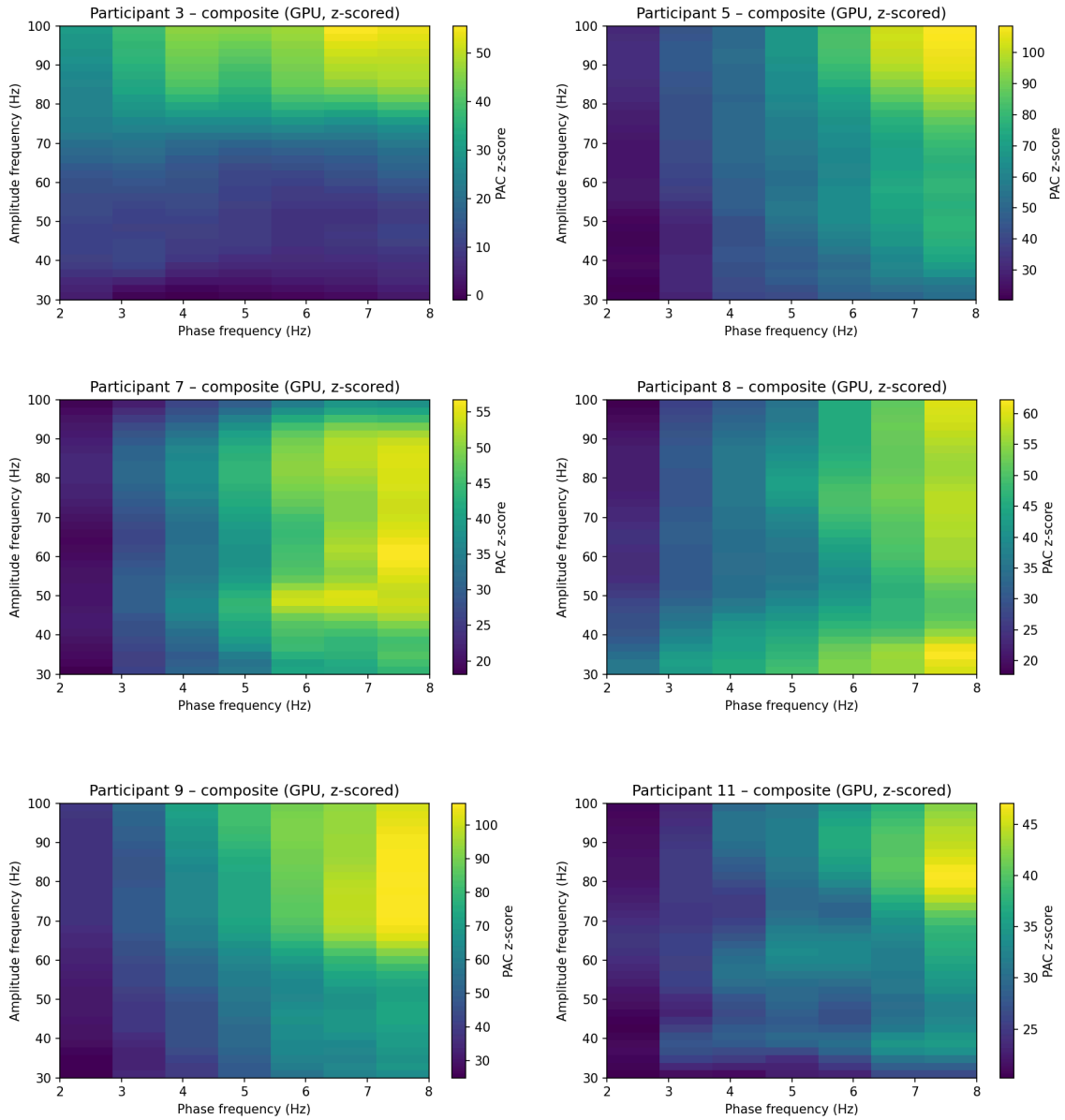

Figure 3.28

Z-scored phase-amplitude coupling (PAC) comodulograms computed using Morlet wavelet convolution and normalized using trial-shuffled surrogates. Results are shown for the composite signal of channel 1 (Ch1) and channel 2 (Ch2).

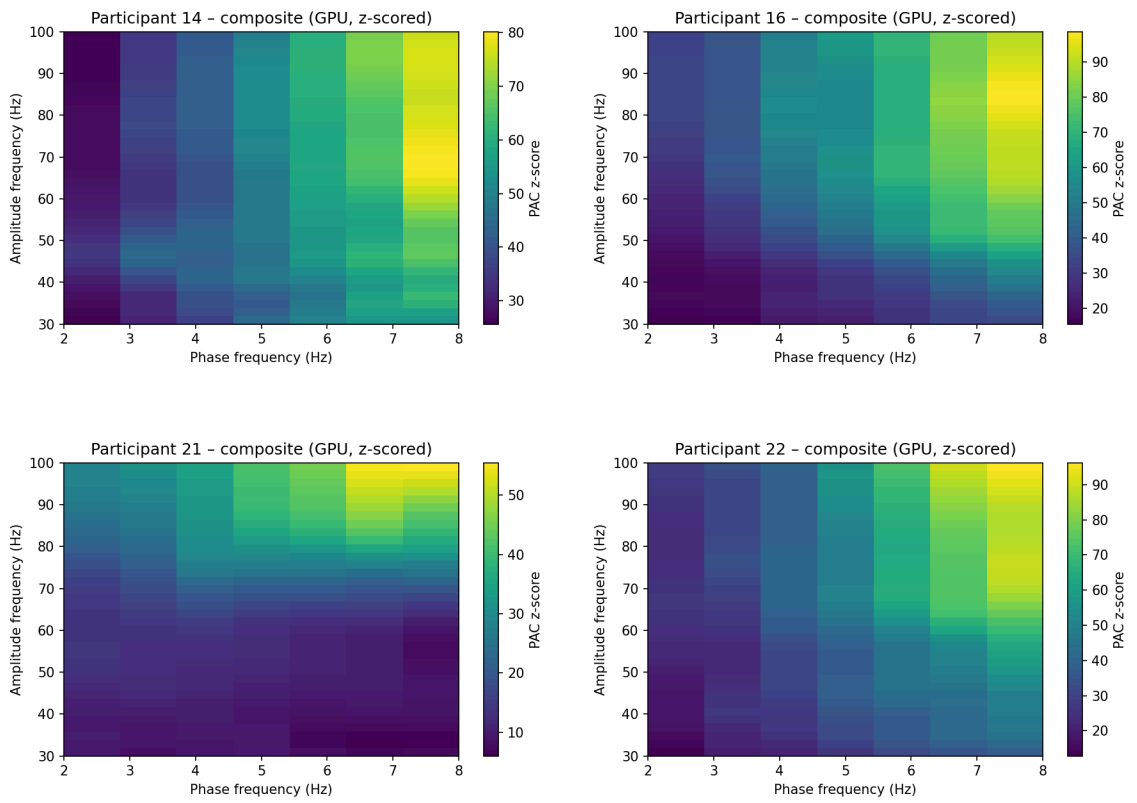

Figure 3.29

Z-scored phase-amplitude coupling (PAC) comodulograms computed using Morlet wavelet convolution and normalized using trial-shuffled surrogates. Results are shown for the composite signal of channel 1 (Ch1) and channel 2 (Ch2).

3.14.3 Highest Phase Frequency Identification and Corresponding Median PAC Computation

To determine which low-frequency phase most strongly modulated high-frequency amplitude activity, we analyzed the z-scored PAC comodulograms obtained from the GPU-based Tort Modulation Index analysis. For each participant and EMG channel (Ch1, Ch2, and composite), the comodulogram matrix (amplitude frequencies × phase frequencies) was set to the 30-100 Hz amplitude range. Within this range, the mean PAC value was calculated for each phase frequency column (2-8 Hz), resulting in one average PAC value per phase frequency. The phase frequency with the highest mean PAC was identified as the best phase frequency for that participant and condition. Then, for this column, the median PAC value across the 30-100 Hz amplitude frequencies was computed to represent the overall strength of coupling at that phase. This procedure was implemented separately for each participant and EMG signal type, producing a measure of the most prominent phase-amplitude interaction in the analyzed frequency range.

3.15 Correlation Analysis

Following the preceding analyses of spatial synergies and PAC, a correlation analysis was conducted to establish whether the extracted neural and muscular coordination metrics were related to behavioral performance, as reflected by participants' grip force measures. The preceding analyses had shown that muscle coordination and oscillatory coupling patterns varied significantly across individuals, revealing individualized synergy "hubs" and subject-specific PAC frequency profiles. However, these analyses did not determine whether these physiological characteristics translated into measurable differences in behavioral output. Thus, correlation analysis was implemented to assess whether participants with stronger or more structured intermuscular connectivity also exhibited higher or more stable grip force production.

The purpose of this analysis was to test the hypothesis that individual variations in muscle coordination and neural coupling mechanisms contribute to behavioral variability in motor performance. Specifically, the correlation analysis explored whether the degree of intermuscular synergy strength, as captured by the unnormalized "raw" synergy matrices, covaried with mean grip force across participants. Additionally, it assessed whether the magnitude of PAC, derived from channel-specific and composite EMG signals, bore any systematic relationship to behavioral output. Single-channel and composite PAC signals were examined. By correlating these neural measures with the behavioral index of grip performance, the analysis aimed to show how low-frequency modulations and muscle synergy organization jointly influence force control.

Three principal categories of variables were included in the correlation matrix. The first was the participant-level mean grip force, extracted from the behavioral dataset, representing each participant's average force across trials. This variable served as a direct quantitative measure of task performance.

The second variable set comprised raw synergy values derived from the participant-specific spatial synergy matrices. For each participant, the synergy matrix represented muscle-to-muscle coordination based on EMG activity. From these matrices, the median synergy strength for each muscle row was computed, and the muscle exhibiting the highest median value was designated as the best. The synergy strength corresponding to this muscle was then used in the correlation analysis as a neural measure of coordination. This ensured that the synergy variable reflected each participant's most representative and functionally relevant coordination feature.

The third group of variables came from the Phase-Amplitude Coupling analyses. For each participant, median PAC values were extracted for both the first and second EMG channels (Ch1 and Ch2) as well as for the composite signal combining both channels. PAC was included to test whether neural oscillatory coordination mirrored or influenced behavioral control and whether stronger intermuscular coupling was accompanied by more efficient or forceful grip output.

By correlating these metrics, grip force, raw synergy, and PAC (Ch1, Ch2, and composite), the analysis aimed to determine whether common underlying mechanisms linked muscular coordination and neural rhythmic modulation to performance variability.

Table 3.4

Participant-level summary of synergy, grip force, and PAC measures used for correlation analysis.

Participant	Synergy best muscle	Mean force	Median PAC composite	Median PAC ch1	Median PAC ch2
1	0.04059	10.21879			
3	0.30161	11.02296	18.36829	0.08115	65.00056
4	0.06556	16.07370			
5	1.27842	13.16737	87.51359	87.11343	92.92398
6	0.14497	15.34296			
7	1.19605	10.88286	51.85782	4.11871	58.73360
8	1.34097	10.52573	60.95348	87.59300	14.43649
9	0.66083	11.20709	93.17982	117.40392	84.29901
10	0.06488	12.33038			
11	0.82580	12.19292	40.29368	0.83042	81.33759
12	0.06449	10.92575			
13	0.03182	11.64273			
14	0.71784	9.68226	73.43832	64.45690	38.91715
16	1.19012	10.21541	87.17255	42.82746	111.67879
21	0.41799	11.09831	14.53822	8.36105	78.08559
22	1.09819	13.02464	69.57384	98.94060	79.18488

Two complementary correlation coefficients were employed, the Pearson correlation and the Spearman rank correlation. The Pearson coefficient quantifies the strength and direction of linear relationships between two continuous variables. It assumes normally distributed data and equal variances across observations. Given that some of the synergy and PAC measures were approximately continuous and near-normally distributed across participants, Pearson's correlation provided an appropriate first test for assessing proportional relationships, whether increases in synergy magnitude linearly corresponded to increases in mean grip force.

The Spearman rank correlation was employed as a non-parametric alternative, capturing monotonic relationships that may not be strictly linear. This approach was used because inter-participant variability in both EMG-derived and behavioral measures often deviates from normality, and small sample sizes can amplify the influence of outliers. Spearman's method ranks data rather than relying on their raw magnitudes, making it more suitable for non-normal distributions and non-linear trends. Using both coefficients allowed for a comprehensive evaluation of the data, balancing sensitivity to linear trends (Pearson) with robustness to outliers and skewed distributions (Spearman).

Given the low number of participants and the potential influence of individual outliers, a Leave-One-Out (LOO) cross-validation procedure was incorporated to assess the stability and reliability of the correlation estimates. In this procedure, correlations were recomputed repeatedly while systematically omitting one participant at a time (O'Reilly and Delis, 2024). This approach tested whether the overall correlation pattern was driven by a small subset of individuals or whether it reflected a consistent trend across the full dataset. If the exclusion of a single participant substantially altered the correlation coefficient, it suggested that the relationship might be unstable or sensitive to that individual's data. Conversely, if the correlation remained relatively unchanged across iterations, it provided evidence that the association was robust.

To further quantify the uncertainty and reliability of the correlation coefficients, bootstrap confidence intervals (CIs) were calculated. Confidence intervals provide a probabilistic range within which the true population correlation is expected to lie, offering a more informative statistical measure than *p*-values alone. In this analysis, 95% CIs were computed by resampling the participant-level data with replacement across multiple iterations. The resulting CI bounds allowed for the distinction between statistically strong, moderate, and weak relationships. If the CI excluded zero, it indicated that the correlation was statistically meaningful at the group level, whereas CIs overlapping zero suggested that the relationship could be due to sampling variability.

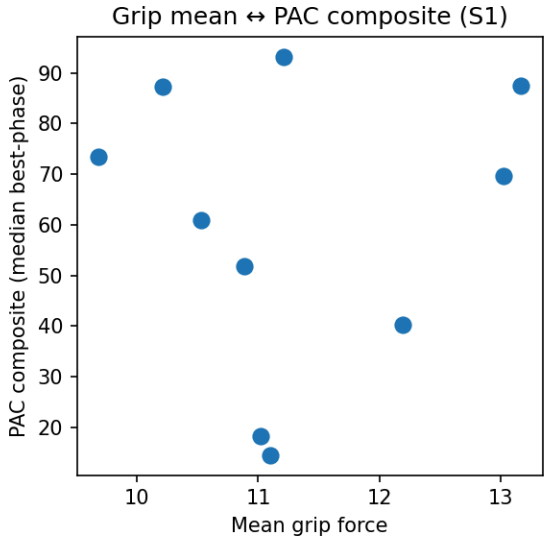

Figure 3.30
Scatterplot showing the relationship between mean grip force and PAC composite values (r = 0.07, p = 0.86).

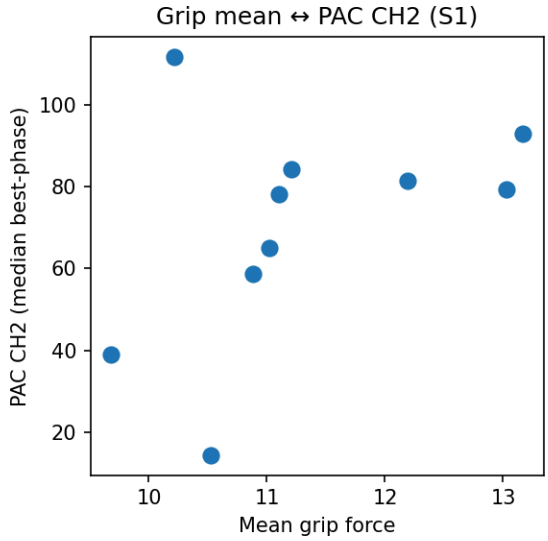

Figure 3.31
Scatterplot showing the relationship between mean grip force and PAC Ch2 values (r = 0.42, p = 0.23).

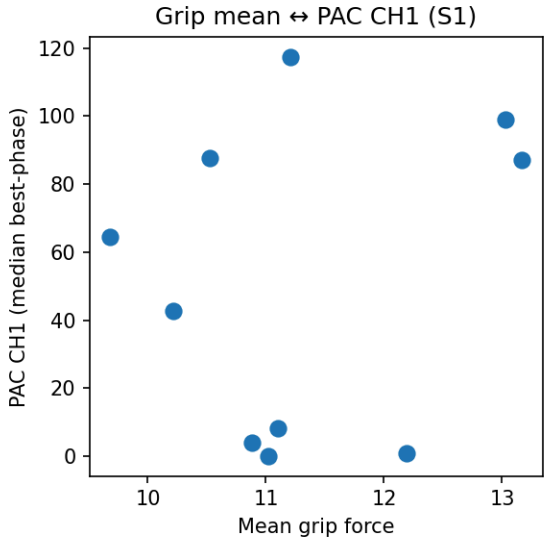

Figure 3.32
Scatterplot showing the relationship between mean grip force and PAC Ch1 values (r = 0.21, p = 0.56).

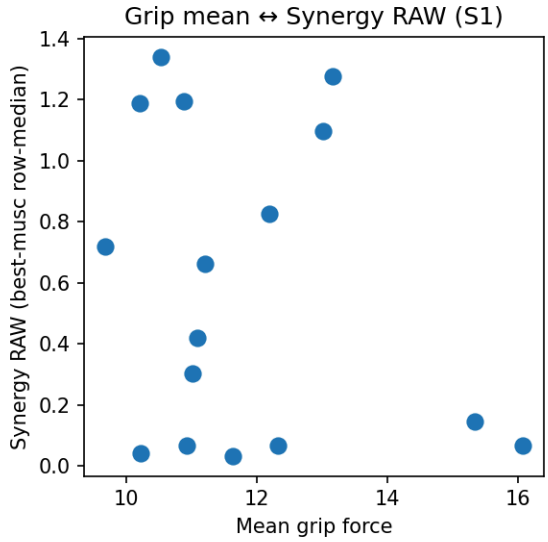

Figure 3.33
Scatterplot showing the relationship between mean grip force and Synergy RAW (r = –0.25, p = 0.35).

CHAPTER 4

RESULTS

4.1 Interpretation of Redundancy Patterns

No measurable redundancy was detected between any recorded muscle pairs during the grip force task. This absence of redundant coupling indicates that, within this dataset and task context, individual muscles contributed largely distinct information to the generation of force, rather than sharing overlapping task-relevant activity patterns. This might be a result of the task-specific nature of precision grip, where the central nervous system constrains motor output to a limited set of highly specialized muscle activations, minimizing variability across redundant pathways. Alternatively, the absence of redundancy could stem from the inherent biomechanical structure of the hand, in which tendon coupling and finely tuned neural control reduce the need for overlapping activation.

Kutch & Valero-Cuevas (2011) demonstrated that *muscle redundancy does not always imply robustness*. In systems like the hand, certain grip-force configurations actually eliminate redundancy because the biomechanical constraints, tendon routing, joint coupling, make the system *overdetermined*. In grip tasks, if muscles act through coupled tendons or if a subset dominates force output, the system may exhibit *apparent or actual non-redundancy*.

Van Bolhuis (1999) showed that redundancy is *task-dependent*. During isometric force tasks, EMG coordination simplifies, muscles reduce co-variation, and redundancy may drop to near zero because the CNS constrains the solution space. A “lack of redundancy” may reflect the nervous system’s optimization.

O’Reilly and Delis (2022) note that redundancy detection depends on mutual information thresholds and co-information estimation.If the task variable has low variability or poor signal-to-noise ratio, the model may underestimate redundancy. Similarly, dimensionality reduction or preprocessing (rectification, filtering, normalization) can suppress shared information between muscle pairs. No redundancy may appear when EMG signals are too noisy or temporally misaligned, the task variable is constant, or the co-information estimation eliminates weak correlations.

Korol & Gritsenko (2024) report that muscle synergies can fail to solve the redundancy problem, especially in tasks with strong biomechanical coupling or limited sensory feedback. They argue that redundancy disappears when motor control is *task-constrained* to a single optimal activation pattern, or when the CNS prioritizes efficiency and stability over flexibility.

4.2 Interpretation of Spatial Synergy Patterns

The synergy analysis revealed consistent and interpretable coordination patterns among muscles during the grip force task. Before normalization, nearly every participant displayed at least one dominant synergy column, a single muscle showing high synergistic coupling with several others. This pattern indicates the presence of a functional hub muscle within each participant's motor network, one whose activity contributed complementary, task-relevant information to multiple other muscles during force generation. In a few cases, participants exhibited either two moderately high synergy columns or scattered synergy "squares," suggesting less centralized coordination. These observations already pointed to individualized but structured patterns of motor organization across participants.

After z-scoring the synergy matrices to normalize for inter-individual differences in EMG scaling, these patterns became even clearer and more distinct. The normalization enhanced contrast within each participant's muscle synergy structure, emphasizing one predominant muscle with consistently high synergy values relative to others. Notably, the identity of this highly synergistic muscle varied between participants, despite all performing the same grip task. This variability suggests that participants employed individualized coordination strategies, recruiting different muscles as central hubs in achieving the same behavioral goal. Such inter-individual variability aligns with previous evidence that the central nervous system can achieve task equivalence through multiple, equally effective coordination patterns.

Hug (2011) discusses how EMG-based synergy analysis reflects functional coordination strategies rather than direct neural commands. He emphasizes that identifying a dominant muscle or "synergy hub" does not necessarily indicate a fixed neural module, but rather a task-dependent adaptation of muscle recruitment to achieve stable performance.Scano and Lanzani (2024) used synergy decomposition in athletes and found that while core muscle synergies were consistent across individuals, the dominant synergistic muscles varied depending on personal technique and biomechanical strategy. Safavynia and Torres-Oviedo (2011) identified multi-muscle synergy structures in upper limb movements and interpreted them as functional modules that simplify motor control. However, they also observed variability in which muscle contributed most to a synergy. De Rugy (2013) questioned the fixed modularity of muscle synergies and suggested that observed patterns may arise from computational optimization within biomechanical constraints rather than rigid neural modules. A single muscle's high synergy across others may represent a computationally optimal coordination solution and not a fixed anatomical pattern.

Furthermore, a subset of participants displayed no discernible synergy after z-scoring, implying weak or inconsistent task-related coupling relative to the group average. These individuals were therefore excluded from subsequent PAC analyses to maintain interpretative validity. Overall, the results indicate that during grip force production, coordination is characterized by a dominant, participant-specific muscle acting as a synergistic hub linking functionally complementary muscles, rather than by a common, group-wide synergy structure. This finding supports that grip control emerges from individualized, structured synergy architectures, emphasizing the adaptability of motor coordination across individuals performing the same task.

4.3 Interpretation of Temporal Synergy Patterns

The analysis of temporal synergies revealed distinct coordination profiles across participants, indicating inter-individual variability in the timing of muscle coactivation during grip force production. Three participants exhibited consistently high temporal synergy across all time windows, indicating globally synchronized muscle activation patterns maintained throughout the task. This pattern likely reflects a stable and cohesive motor command, where muscles are temporally coupled over the entire duration of force generation, potentially a well-learned or automatized control strategy.

In contrast, eight participants showed minimal or near-zero temporal synergy across all time windows, suggesting a more independent or decoupled control of muscle activations. The observation that several participants exhibited near-zero temporal synergy across all time windows is consistent with prior evidence suggesting that muscles can operate largely independently under certain task conditions. Maier & Hepp-Reymond (1995) first showed that precision grip involves partially decoupled muscle activations to allow fine force adjustments. Similarly, Delis et al. (2018) and Esmaeili & Maleki (2020) reported that low temporal synergy reflects flexible, task-specific modulation. Neural studies, such as Laine & Cohn (2021), suggest that the modulation of cortical synchrony allows adaptive temporal decoupling across muscles depending on force demands.

A smaller subset of participants demonstrated time-specific synergy patterns. Three participants displayed high temporal synergy toward the end of the trial (time windows 15-20), suggesting an increased coupling during force stabilization or release phases, consistent with prior evidence that temporal coherence between muscles increases during force maintenance or the deceleration phase of movement (Hug et al., 2011; Safavynia and Torres-Oviedo, 2011). Conversely, two participants exhibited synergy early in the task (time windows 1-15), corresponding to force onset and ramp-up, a phase characterized by dynamic recruitment and rapid coordination of agonists and stabilizers.

These results indicate that while some participants maintain stable, globally synchronized muscle timing throughout the task, others exhibit phase-specific coordination aligned with distinct motor components, such as grip initiation or stabilization. The heterogeneity across individuals shows the flexible nature of temporal motor control, suggesting that temporal synergies, like spatial ones, are individualized and reflect multiple viable timing solutions for achieving the same behavioral goal.

4.4 Phase-Amplitude Coupling Results

Phase-amplitude coupling (PAC) analysis was conducted to examine whether low-frequency oscillations modulate the amplitude of higher-frequency activity within and across synergistic muscles during grip force control. Two separate analyses were implemented to validate the coupling patterns, a MATLAB-based computation using Hilbert-transform derived analytic signals and a GPU-accelerated Python implementation employing complex Morlet wavelet convolution with surrogate-based normalization.

4.4.1 MATLAB Hilbert Angle based PAC

In the MATLAB analysis, PAC comodulograms computed with the Tort Modulation Index revealed consistent modulation patterns across all participants and channels. Both single-channel and composite-channel comodulograms showed pronounced coupling between the 2 Hz phase frequency and high-frequency amplitude components spanning the 30-100 Hz range. This effect was evident in both the raw and z-scored comodulograms, indicating that slow oscillations around 2 Hz systematically modulated the envelope of high-frequency EMG activity.

The high Modulation Index (MI) values observed at 2 Hz were consistent across participants, leading to the selection of the 2 Hz phase frequency as the region of interest (ROI) for subsequent quantitative analysis. Median MI values calculated within this ROI confirmed that 2 Hz represented the dominant low-frequency driver of high-frequency amplitude modulation. The similarity of these results across participants and across both raw and composite signals suggested a stable underlying modulation mechanism, showing slow control rhythms modulating muscle activation bursts.

However, this apparent consistency must be interpreted with caution. The MATLAB PAC analysis did not include surrogate-based statistical correction, meaning that the observed coupling could partially reflect non-neural effects such as slow drifts, filter edge artifacts, or the inherent envelope correlation between amplitude and phase signals derived from the same data. Consequently, the high uniform PAC values at 2 Hz may represent an overestimation of true cross-frequency coupling strength.

Table 4.1

Comparison of median PAC and median composite PAC values across participants and channels for the selected ROI, (phase frequency=2 Hz).

Participant	Channel	PAC Median	Composite channel	Composite PAC Median
3	7	0.010	7 - 9	0.010
3	9	0.011		
5	3	0.015	3 - 9	0.009
5	9	0.010		
7	1	0.030	1 - 9	0.010
7	9	0.009		
8	1	0.016	1 - 9	0.013
8	9	0.041		
9	5	0.016	5 - 9	0.010
9	9	0.011		
11	7	0.006	7 - 9	0.008
11	9	0.014		
14	2	0.014	2 - 3	0.010
14	3	0.014		
16	6	0.013	6 - 9	0.010
16	9	0.011		
21	8	0.016	8 - 5	0.009
21	5	0.010		
22	4	0.009	4 - 9	0.008
22	9	0.010		

4.4.2 Python Morlet Wavelet Convolution - Surrogate PAC

To address these concerns, a second PAC analysis was performed in Python using Morlet wavelet convolution for time-frequency decomposition and a surrogate-based normalization procedure to assess statistical significance. This method preserved the same frequency ranges (2-8 Hz phase; 30-100 Hz amplitude) and employed the Tort Modulation Index but introduced trial-shuffled surrogates (n = 200) to derive z-scored PAC maps.

The resulting comodulograms differed markedly from those obtained via the MATLAB analysis. Instead of a uniform dominance of 2 Hz across all participants, the best phase frequency varied substantially between subjects and channels, with most peak PAC occurring in the 6-8 Hz range. Table 4.2 summarizes these individual maxima, showing that no consistent ROI emerged across participants. Furthermore, the range of z-scored PAC values was broader, indicating increased sensitivity to inter-participant and channel-specific differences once chance-level coupling was statistically controlled.

This discrepancy between MATLAB and Python results likely shows both methodological and statistical factors. The Morlet wavelet method has improved temporal precision and captures transient oscillatory interactions that narrowband Hilbert filters tend to smooth out. Moreover, the inclusion of surrogate-based normalization effectively removes coupling due to signal autocorrelation or amplitude bias, yielding a more conservative but physiologically reliable estimate of PAC strength. The apparent uniformity of the 2 Hz coupling in the MATLAB results was likely due to methodological bias rather than a true neural effect.

Table 4.2
Best phase frequency (2-8 Hz) and corresponding median z-scored PAC for each participant and EMG condition (Ch1, Ch2, composite).

Participant	Ch1 best phase	Ch1 median PAC	Ch2 best phase	Ch2 median PAC	Composite best phase	Composite median PAC
3	6	0.081	8	65.001	8	18.368
5	8	87.113	8	92.924	8	87.514
7	2	4.119	8	58.734	8	51.858
8	8	87.593	5	14.436	8	60.953
9	8	117.404	8	84.299	8	93.180
11	6	0.830	8	81.338	8	40.294
14	8	64.457	8	38.917	8	73.438
16	8	42.827	8	111.679	8	87.173
21	8	8.361	8	78.086	7	14.538
22	8	98.941	8	79.185	8	69.574

Table 4.2 lists, for each participant, the phase frequency (2-8 Hz) that produced the highest phase-amplitude coupling (PAC) within the 30-100 Hz amplitude range, along with the median z-scored Tort modulation index (PAC strength) at that frequency. Values are shown separately for the first EMG channel (Ch1), second EMG channel (Ch2), and their composite signal.

4.5 Comparison and Interpretation

While the MATLAB Hilbert-based analysis identified a seemingly stable low-frequency modulator (2 Hz) across all subjects, the Python wavelet-based approach revealed participant-specific coupling structures with no universal ROI, suggesting that the true coupling dynamics are more variable and context-dependent.

The absence of a consistent 2 Hz phase driver implies that low-frequency modulation of high-frequency EMG activity is not governed by a single oscillatory process but instead arises from multiple components that may differ between muscles and individuals.

Therefore, the earlier conclusion that 2 Hz represented a uniform global modulator should be considered as a methodological artifact of the non-surrogate PAC approach. Nonetheless, the broader finding that slow oscillatory phases modulate high-frequency muscle activity remains valid, as evidenced by the significant PAC detected across multiple frequency pairs in the surrogate-corrected results.

4.6 Pearson - Spearman Correlation between Synergy and Grip Force

Table 4.3

Correlation analysis results (Pearson and Spearman) for the relationship between Synergy and grip force.

Pearson Correlation	
n	16
Pearson r	-0.2521
Pearson p	0.3462
Pearson CI lower bound	-0.6117
Pearson CI upper bound	0.3561
Pearson LOO lower bound	-0.3532
Pearson LOO upper bound	-0.1061

Spearman Correlation	
n	16
Spearman r	-0.1559
Spearman p	0.5643
Spearman CI lower bound	-0.6107
Spearman CI upper bound	0.4045
Spearman LOO lower bound	-0.3036
Spearman LOO upper bound	-0.0571

The correlation analysis between synergy and grip force revealed no statistically significant linear or monotonic association. The Pearson correlation coefficient (r = –0.2521, p = 0.3462, n=16) indicated a weak, negative linear relationship that was not statistically significant. The 95% confidence interval for the Pearson correlation (–0.6117 to 0.3561) included zero, suggesting that the true correlation could range from moderately negative to moderately positive. Similarly, the Spearman rank correlation coefficient (ρ = –0.1559, p = 0.5643) indicated the absence of a significant monotonic relationship between the variables. The leave-one-out (LOO) cross-validation analysis showed that both the Pearson LOO bounds (–0.3532 to –0.1061) and Spearman LOO bounds (–0.3036 to –0.0571) remain weak and negative, consistent with the direction of the overall correlation (weakly negative). The consistency across LOO estimates indicates that the correlation remains weak regardless of which data point is removed, and the weak relationship is not driven by a single outlier.

4.6.1 Linear Regression between Synergy and Grip Force

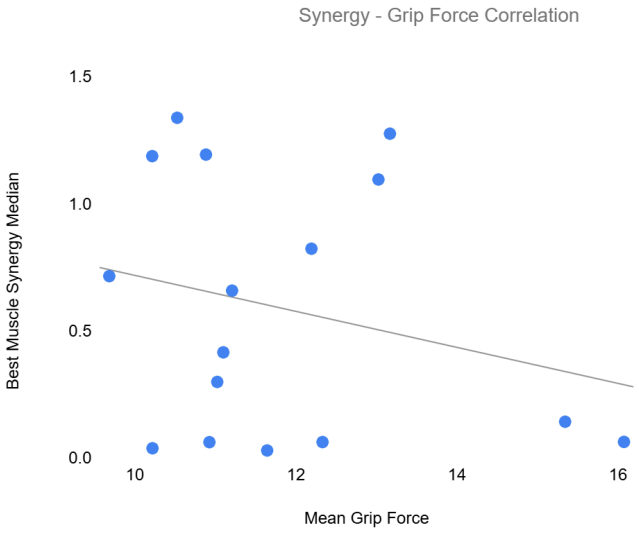

Linear Regression	
Pearson R^2	0.0636
Slope	-0.0708
Intercept	1.4293

Figure 4.1
Linear regression between synergy and grip force.

In the linear regression analysis, synergy was modeled as a function of grip force, yielding a coefficient of determination (R^2 = 0.0636), a slope of –0.0708, and an intercept of 1.4293. This R^2 value indicates that only approximately 6.4% of the variance in synergy can be explained by grip force, which is considered negligible. The negative slope suggests a slight decrease in synergy with increasing grip force. However the correlation is weak and the p-value is not significant. This relationship could be due to random variation rather than a true underlying effect.

4.7 Pearson - Spearman Correlation between Composite Channel PAC and Grip Force

Table 4.4
Correlation analysis results (Pearson and Spearman) for the relationship between composite channel phase-amplitude coupling (PAC) and grip force.

Pearson Correlation	
n	10
Pearson r	0.0664
Pearson p	0.8554
Pearson CI lower bound	-0.5886
Pearson CI upper bound	0.5807
Pearson LOO lower bound	-0.1702
Pearson LOO upper bound	0.2032

Spearman Correlation	
n	10
Spearman r	0.0667
Spearman p	0.8548
Spearman CI lower bound	-0.7274
Spearman CI upper bound	0.6154
Spearman LOO lower bound	-0.2333
Spearman LOO upper bound	0.2000

The correlation analysis between the composite channel PAC and grip force signals indicated no statistically significant association. The Pearson correlation coefficient (r=0.0664, p=0.8554, n=10) revealed an extremely weak positive linear relationship, with the 95% confidence interval (–0.5886 to 0.5807) including zero. This broad interval suggests uncertainty regarding the direction and strength of the relationship. The Spearman rank correlation coefficient (ρ=0.0667, p=0.8548) indicated an equally weak monotonic association. The wide confidence intervals further show the absence of a reliable trend.

The leave-one-out (LOO) cross-validation bounds for both Pearson (–0.1702 to 0.2032) and Spearman (–0.2333 to 0.2000) correlations were wide and crossed zero. This indicates that the correlation coefficient varied considerably depending on which participant was excluded from the analysis, with the direction of the relationship shifting between slightly negative and slightly positive. The large relative width of the LOO ranges demonstrates that the estimated correlations are highly unstable and not robust. Therefore, the results suggest that the relationship between the composite channel PAC and grip force is weak, inconsistent, and likely driven by random variation.

4.7.1 Linear Regression between Composite Channel PAC and Grip Force

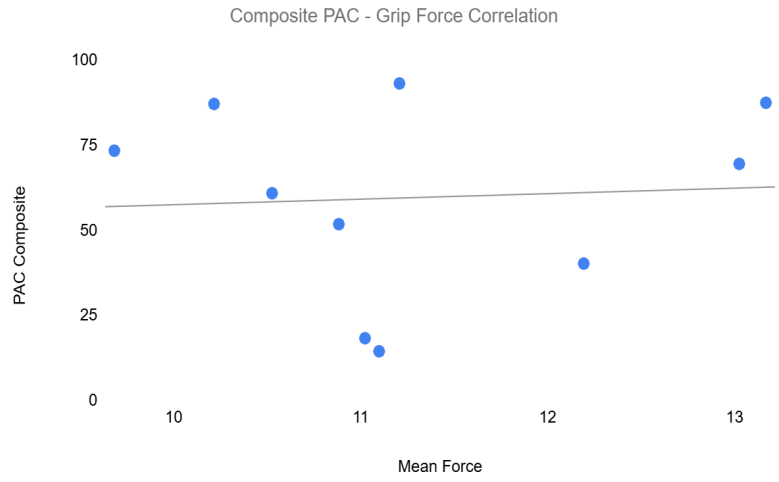

Linear Regression	
Pearson R^2	0.0044
Slope	1.6204
Intercept	41.3752

Figure 4.2
Linear regression between composite channel phase-amplitude coupling (PAC) and grip force.

The linear regression analysis, modeling the composite channel PAC as a function of grip force, produced an R^2 value of 0.0044, a slope of 1.6204, and an intercept of 41.3752. The R^2 indicates that only about 0.4% of the variance in composite PAC values can be explained by grip force, signifying negligible explanatory power. Although the regression slope was positive, the combination of the small R^2 and nonsignificant correlation indicates that this trend is likely random rather than systematic.

The results demonstrate no meaningful linear or monotonic relationship between the composite channel PAC and grip force signals. The weak correlations and minimal explained variance in the regression model indicate that changes in grip force do not predict changes in the composite channel PAC under the conditions examined.

4.8 Pearson - Spearman Correlation between Channel 1 PAC and Grip Force

Table 4.5

Correlation analysis results (Pearson and Spearman) for the relationship between Channel 1 phase-amplitude coupling (PAC) and grip force.

Pearson Correlation	
n	10
Pearson r	0.2117
Pearson p	0.5570
Pearson CI lower bound	-0.6223
Pearson CI upper bound	0.6875
Pearson LOO lower bound	0.0233
Pearson LOO upper bound	0.3575

Spearman Correlation	
n	10
Spearman r	0.1879
Spearman p	0.6032
Spearman CI lower bound	-0.5502
Spearman CI upper bound	0.6376
Spearman LOO lower bound	-0.0333
Spearman LOO upper bound	0.3500

The correlation analyses between channel 1 PAC and grip force signals showed a weak, non-significant positive association. The Pearson correlation coefficient (r =0.2117, p=0.5570, n =10) indicated a small positive linear trend between Channel 1 PAC values and grip force, but the relationship was not statistically significant. The 95% confidence interval (–0.6223 to 0.6875) included both negative and positive values. Similarly, the Spearman rank correlation coefficient (ρ = 0.1879, p = 0.6032) suggested a weak monotonic relationship that was not significant, with a wide confidence interval (–0.5502 to 0.6376) including zero.

The Pearson correlation between Channel 1 PAC and grip force is directionally stable and relatively stable in magnitude, indicating that no single participant drives the correlation or causes it to flip direction. However, the correlation itself is weak and statistically not significant. The Spearman correlation is weak and directionally inconsistent, suggesting that a few data points have a disproportionate influence. This instability implies that the monotonic relationship between Channel 1 PAC and grip force is not robust and may be affected by outliers or small-sample variability.

4.8.1 Linear Regression between Channel 1 PAC and Grip Force

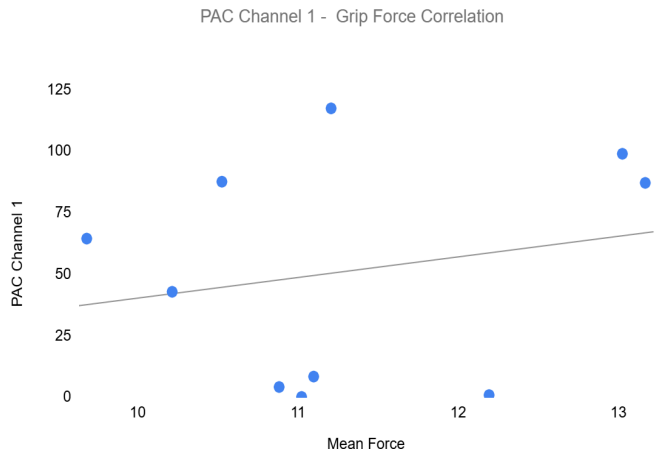

Linear Regression	
Pearson R^2	0.0448
Slope	8.3812
Intercept	-43.5516

Figure 4.3
Linear regression between channel 1 phase-amplitude coupling (PAC) and grip force.

In the linear regression analysis, Channel 1 PAC was modeled as a function of grip force, yielding a coefficient of determination (R^2 = 0.0448), a slope of 8.3812, and an intercept of –43.5516. The R^2 value indicates that only about 4.5% of the variance in Channel 1 PAC values can be explained by grip force. Although the regression slope was positive, suggesting that higher grip force values may be associated with slightly higher Channel 1 PAC values, the overall effect was weak and statistically non-significant.

In summary, the results demonstrate that Channel 1 PAC and grip force show a weak, non-significant positive association. The low correlation coefficients, wide confidence intervals, and minimal explained variance suggest that changes in grip force do not meaningfully predict Channel 1 PAC signals.

4.9 Pearson - Spearman Correlation between Channel 2 PAC and Grip Force

Table 4.6

Correlation analysis results (Pearson and Spearman) for the relationship between Channel 2 phase-amplitude coupling (PAC; deltoid muscle) and grip force.

Pearson Correlation	
n	10
Pearson r	0.4164
Pearson p	0.2313
Pearson CI lower bound	-0.2744
Pearson CI upper bound	0.9066
Pearson LOO lower bound	0.2751
Pearson LOO upper bound	0.7315

Spearman Correlation	
n	10
Spearman r	0.4909
Spearman p	0.1497
Spearman CI lower bound	-0.3251
Spearman CI upper bound	1.0000
Spearman LOO lower bound	0.3333
Spearman LOO upper bound	0.9167

The correlation analysis between Channel 2 PAC and grip force revealed a moderate but statistically non-significant positive association. The Pearson correlation coefficient ($r = 0.4164$, $p = 0.2313$, $n = 10$) suggested a moderate positive linear relationship, indicating that higher grip force values were generally associated with higher Channel 2 values, but the relationship was not statistically significant. The 95% confidence interval (–0.2744 to 0.9066) was wide and crossed zero, indicating uncertainty due to the small sample size.The Spearman rank correlation coefficient ($\rho = 0.4909$, $p = 0.1497$) showed a similar monotonic trend, also in the positive direction, though still not statistically significant. The confidence interval (–0.3251 to 1.0000) was wide and crossed zero.

The leave-one-out (LOO) analysis demonstrated relatively stable and consistently positive correlations for both Pearson (0.2751 to 0.7315) and Spearman (0.3333 to 0.9167) correlation coefficients. This consistency suggests that, while the effect size fluctuates with the removal of individual observations, the overall positive direction of the relationship is not driven by outliers.

4.9.1 Linear Regression between Channel 2 PAC and Grip Force

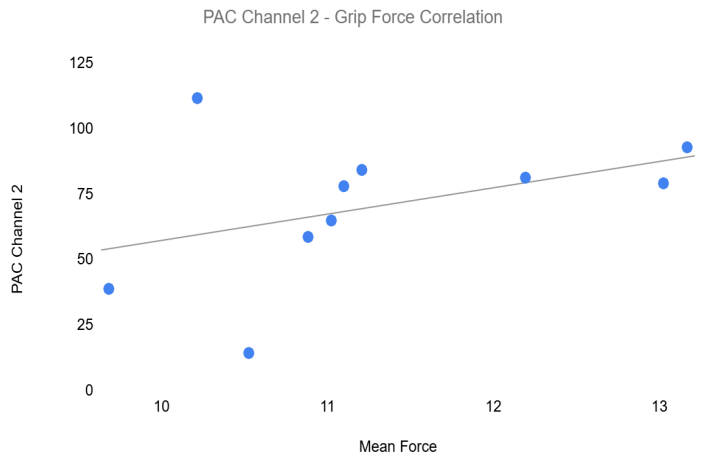

Linear Regression	
Pearson R^2	0.1734
Slope	10.0395
Intercept	-43.0060

Figure 4.4
Linear regression between channel 2 phase-amplitude coupling (PAC) and grip force.

The linear regression analysis, modeling Channel 2 PAC as a function of grip force, yielded an R^2 value of 0.1734, a slope of 10.0395, and an intercept of –43.0060. The R^2 indicates that approximately 17.3% of the variance in Channel 2 PAC can be explained by grip force, substantially higher than in the other PAC-grip force relationships, though still relatively modest. The positive slope supports the interpretation that increases in grip force are accompanied by corresponding increases in Channel 2 PAC values, albeit with limited predictive power given the lack of statistical significance.

The findings suggest a potential moderate positive relationship between PAC Channel 2 and grip force signals. Although not statistically significant, the consistent positive direction across both correlation methods and LOO validation shows an underlying association that may become clearer with a larger sample size. These results indicate that Channel 2 PAC may be more functionally sensitive to grip force modulation than the other PAC measures examined, but further research with greater statistical power is required to confirm this relationship.

Considering that Channel 2 primarily represented EMG signals from the deltoid muscle for most participants, the positive correlation observed between Channel 2 PAC and grip force may reflect a degree of coactivation during grip tasks. Although the correlations were moderate in strength (Pearson r = 0.4164, Spearman ρ = 0.4909) and not statistically significant, both measures exhibited directionally stable and positive LOO bounds, suggesting a consistent tendency for higher deltoid PAC values with greater grip force.

4.10 Correlation Analysis Overview

The Pearson correlation between mean grip force and the composite PAC (r = 0.066, p = 0.855) was near zero, and similar results were obtained for PAC from Ch1 (r = 0.21, p = 0.56). In

contrast, the PAC from Ch2 showed a moderate positive trend ($r = 0.42$, $p = 0.23$), although not statistically significant. This pattern suggests that while there may be a tendency for increased coupling strength at Ch2 to associate with higher grip force, the relationship is not robust across participants. The Spearman correlations mirrored this trend, with Ch2 showing the highest monotonic relationship ($\rho = 0.49$, $p = 0.15$), indicating that rank-order associations were somewhat stronger than linear ones, though still below conventional significance thresholds.

The raw synergy strength (representing the best muscle row median from the synergy matrix) was negatively correlated with grip force ($r = -0.25$, $p = 0.35$), a direction suggesting that participants with more pronounced intermuscular coupling did not necessarily exhibit stronger behavioral performance. This may reflect compensatory activation or redundancy within the synergy structure, as proposed by O'Reilly and Delis (2024), who argue that excessive coactivation may represent energy-inefficient or redundant control rather than functional coordination.

These findings indicate that PAC and synergy metrics are not directly or linearly predictive of grip force in this dataset. Instead, they may reflect distinct aspects of motor coordination that operate at different levels-synergy metrics capturing the *spatial structure* of muscle coactivation, and PAC metrics capturing *temporal modulation* and rhythmic synchronization. This conceptual dissociation aligns with recent studies emphasizing that synergy-derived metrics and oscillatory coupling represent complementary mechanisms rather than redundant ones (Zhao et al., 2023; De Bei, 2025).

The Leave-One-Out (LOO) intervals indicated that correlation estimates were stable across participants, with minimal changes in directionality when individual data points were removed. This supports the reliability of the weak-to-moderate correlations observed, even though their magnitudes were not significant. Similarly, bootstrap confidence intervals (CIs) were wide for all metrics, reflecting uncertainty due to the small sample size but also suggesting that both weak and moderate associations are plausible in the broader population.

In small-N behavioral neuroscience studies, even moderate correlations ($|r| \approx 0.4$-0.5) can represent meaningful physiological trends, as shown in prior EMG-based investigations of hand synergies (Rinaldi, 2020; Wochner, 2023). Thus, while our findings fall below statistical significance, their consistency and directionality provide preliminary evidence for differentiated roles of synergy and PAC measures in modulating behavioral performance.

The negative correlation between raw synergy strength and grip force could imply that participants with stronger baseline muscle coactivation did not necessarily perform better. This observation resonates with findings from *De Bei (2025)*, who reported that excessive intermuscular synergy strength may indicate reduced independence among muscles, potentially constraining fine control during precise movements. This interpretation aligns with the redundant coupling hypothesis of O'Reilly and Delis (2024), suggesting that higher synergy strength may reflect over-constrained motor coordination, sacrificing flexibility and adaptability

CHAPTER 5

DISCUSSION AND CONCLUSION

5.1 General Overview

This study investigated how redundant and synergistic muscle coordination contributes to grip force control and examined how these coordination structures relate to cross-frequency coupling in EMG signals. By integrating information-theoretic decomposition with PAC analyses, this work aimed to uncover hierarchical relationships between spatial and temporal muscle synergies and oscillatory modulation mechanisms underlying grip control. The results revealed three main findings, minimal measurable redundancy between muscles during grip tasks, individualized but structured synergy patterns characterized by dominant “hub” muscles, and the presence of low-frequency phase modulation of high-frequency EMG components, detected through surrogate PAC analysis. These findings suggest that the central nervous system achieves stable and adaptable grip control through individualized, synergy structures modulated by slow oscillatory drives. This supports the view of motor coordination as a hierarchical and flexible system, rather than one relying on fixed neural modules or overlapping redundancy.

5.2 Redundancy and the Efficiency of Motor Control

The near absence of redundancy across recorded muscle pairs indicates that the CNS minimizes overlapping contributions among muscles when regulating grip force. This observation aligns with prior research showing that redundancy is not universal but instead depends on task constraints and biomechanical configuration (Kutch & Valero-Cuevas, 2011; Van Bolhuis, 1999). In precision grip, muscles operate within an overdetermined mechanical system where tendon coupling and joint structure limit the range of viable activations. Information decomposition analysis revealed negligible shared information (ST_R) between muscle pairs, suggesting that each muscle encodes largely distinct aspects of the task variable (grip force).

5.3 Spatial Synergy Structure - Individualized Coordination Strategies

Spatial synergy analysis revealed that participants consistently exhibited a single dominant synergy column corresponding to one highly synergistic “hub” muscle. This muscle showed strong, complementary coupling with several others, suggesting its role as a coordination center within the synergy network. However, the identity of this hub muscle varied across individuals, demonstrating flexible recruitment strategies by the CNS to accomplish the same motor objective.

This variability supports the view that muscle synergies are functional rather than anatomical units. As Hug (2011) and Scano & Lanzani (2024) have proposed, synergy patterns reflect

context-dependent coordination strategies rather than fixed neural modules. Each participant's unique synergy configuration may represent an optimized solution to their biomechanical structure, force dynamics, and motor learning history. Safavynia and Torres-Oviedo (2011) also reported that inter-individual differences in synergy weighting reflect personalized adaptations that maintain task-level performance despite variability in neural recruitment patterns.

5.4 Temporal Synergy - Flexible Timing and Adaptation

Temporal synergy results revealed heterogeneous timing patterns across participants. Some exhibited globally synchronized activation patterns, suggesting unified temporal coordination across all muscles, whereas others displayed phase-specific synergy peaks, often concentrated during grip stabilization or release. These differences may reflect the CNS's ability to dynamically reconfigure timing strategies according to task phase, sensory feedback, or fatigue.

Low temporal synergy during certain phases indicates that muscles can operate independently to allow fine adjustments in force output, a feature consistent with Maier & Hepp-Reymond's (1995) demonstration of partial decoupling during precision grip. Delis et al. (2018) and Laine & Cohn (2021) further support this interpretation, showing that temporal variability reflects flexible cortical-muscular coupling tuned to momentary control demands.

5.5 Cross-Frequency Coupling: Oscillatory Modulation of Synergistic Activity

Phase-amplitude coupling analysis revealed that slow oscillations (2-8 Hz) modulated the amplitude of high-frequency EMG activity (30-100 Hz), indicating that hierarchical frequency interactions play a role in shaping muscle coordination. While initial Hilbert-based PAC analyses suggested a uniform 2 Hz modulator, the surrogate-corrected Morlet wavelet results revealed participant-specific dominant frequencies, most often within the 6-8 Hz range.

The significant PAC observed across both single and composite muscle signals implies that synergistically coactive muscles share common oscillatory drives, consistent with previous evidence linking cross-frequency coupling to coordinated motor output (Florin & Baillet, 2015; Canolty et al., 2006). These oscillatory interactions may represent neural control mechanisms that temporally structure synergy recruitment. The theta-range modulation observed in several participants corresponds to the cortical-muscular coherence frequencies associated with motor execution and sensorimotor integration.

5.6 Grip Force and Synergy, and PAC Correlation

The non-significant correlations observed here should not be interpreted as an absence of functional relationships, but rather as evidence that these relationships may be nonlinear, context-dependent, or multi-factorial. For instance, previous work has shown that synergy and PAC dynamics often correlate more strongly with *variability* in force or *adaptation rate* rather than mean force itself (Saheb Jameyan & Ahmadi-Pajouh, 2025). This suggests that future analyses might focus on trial-level variability or spectral coupling changes across time rather than participant-level averages.

5.7 Methodology

Integrating information-theoretic and frequency-domain analyses provided complementary insights into neuromuscular coordination. The mutual information decomposition quantified structural interdependencies, while PAC analysis revealed temporal modulation mechanisms. However, methodological differences between Hilbert and Morlet implementations show the importance of analytic precision in EMG-based CFC studies.

Nevertheless, several methodological considerations warrant caution. EMG signals are influenced by electrode placement, filtering, and normalization choices, all of which can alter synergy dimensionality or PAC magnitude. Additionally, surface EMG cannot directly attribute oscillatory coupling to central neural sources. Future multimodal approaches combining EMG with EEG or MEG could address this limitation by linking peripheral and cortical PAC patterns.

5.8 Limitations

The main limitations of this study include, inter-individual variability in synergy and PAC patterns, which complicates group-level generalization. Absence of neural recordings, restricting conclusions about the cortical origin of observed oscillatory effects. Sample size constraints, which may limit statistical inference on subtle coordination patterns.

Methodologically, the phase-amplitude coupling analysis was performed only on a subset of participants who exhibited strong synergy patterns compared to the group. Consequently, the PAC results may be biased toward individuals with more pronounced coordination, potentially overlooking subtler modulations present in the wider sample. In addition, not all channels were selected for PAC analysis, which may have constrained the diversity of muscle interactions examined.

Another limitation concerns the computation of the composite channel, which was generated using a simple averaging of z-scored signals. While this approach provided a straightforward representation of synergistic muscle activity, it may not have fully captured the underlying nonlinear relationships among muscles. Alternative signal integration strategies, such as weighted combinations or dimensionality reduction methods, could provide a more physiologically meaningful representation of synergy.

Finally, the correlation between temporal synergy and grip force, as well as between PAC modulation and synergy measures, was not directly tested. Examining these relationships could offer a more spherical view of how oscillatory modulation and synergistic muscle coordination jointly influence grip force force control.

5.9 Future Directions

Future work could focus on integrating multimodal neurophysiological recordings, such as combined EEG-EMG or MEG-EMG analyses, to trace the cortical or spinal origins of the peripheral PAC and synergy patterns identified here. This could clarify whether shared neural drives observed at the muscle level reflect genuine modulation from motor cortical areas or peripheral feedback mechanisms.

Methodological refinements could include the application of higher-order information decomposition models, which can capture multidimensional coordination structures that extend beyond pairwise muscle interactions. Such models would enable the simultaneous analysis of spatial, temporal, and frequency-domain dependencies within a unified framework.

Expanding the participant sample could improve statistical robustness and reduce variability across subjects. In addition, future studies could employ more sophisticated approaches for channel selection and composite channel construction, such as synergy-weighted averaging or connectivity-based integration, to better represent functional muscle groupings.

Finally, directly correlating PAC measures with synergy metrics and grip force signals across all participants could yield a more comprehensive understanding of how oscillatory coupling and coordinated muscle activation interact to produce fine motor control. These refinements would advance the quantitative modeling of muscle coordination and potentially support the development of predictive biomarkers for neuromuscular performance and rehabilitation.

5.10 Conclusion

This thesis provides new evidence that muscle coordination during grip force control is governed by individualized synergy structures modulated by low-frequency oscillatory drives. Through the combined application of information decomposition and phase-amplitude coupling analyses, it demonstrates that the central nervous system employs hierarchical, structured mechanisms to achieve efficient and flexible control of synergistic muscle activations.

The spatial synergy results revealed individualized coordination networks, often centered around a primary muscle,most commonly the deltoid, while temporal synergy patterns showed greater diversity and predominated in the early phase of grip control. The absence of redundancy suggests that muscle coordination during this task relies primarily on complementary rather than overlapping neural representations.

Phase-amplitude coupling analysis further indicated that slow oscillatory components modulate high-frequency EMG activity, reflecting potential shared neural drives within the peripheral motor system. Although the correlations between PAC measures and grip force were not statistically significant, the consistent trends, particularly within deltoid-dominated channels, suggest that oscillatory modulation may encode task-relevant information linked to force regulation.

Overall, by connecting the principles of information theory, signal decomposition, and biomechanics, the study contributes to a deeper understanding of motor coordination mechanisms and provides a foundation for developing future models capable of predicting physiological outcomes from EMG signals.

BIBLIOGRAPHY

Berret, B., & Delis, I. (2018). A framework for the analysis of spatiotemporal synergies in multi-muscle coordination. *Frontiers in Computational Neuroscience, 12*, 85. https://doi.org/10.3389/fncom.2018.00085

Birmpas, K. (2024). *Computational neuroscience: Leveraging machine learning techniques to extract neurally informed behavioural signatures* [Master's thesis, University of Patras, Department of Electrical and Computer Engineering].

Bizzi, E., Cheung, V. C. K., d'Avella, A., Saltiel, P., & Tresch, M. (2008). Combining modules for movement. *Brain Research Reviews, 57*(1), 125–133. https://doi.org/10.1016/j.brainresrev.2007.08.004

Canolty, R. T., Edwards, E., Dalal, S. S., Soltani, M., Nagarajan, S. S., Kirsch, H. E., Berger, M. S., Barbaro, N. M., & Knight, R. T. (2006). High gamma power is phase-locked to theta oscillations in human neocortex. *Science, 313*(5793), 1626–1628. https://doi.org/10.1126/science.1128115

Canolty, R. T., & Knight, R. T. (2010). The functional role of cross-frequency coupling. *Trends in Cognitive Sciences, 14*(11), 506–515. https://doi.org/10.1016/j.tics.2010.09.001

Chen, Y., Li, X., & Delis, I. (2025). Redundancy and synergy in neuromuscular coordination: An information-theoretic analysis. *Journal of Neural Engineering, 22*(2), 026015.

Cohen, M. X. (2014). *Analyzing neural time series data: Theory and practice*. MIT Press.

D'Avella, A., & Bizzi, E. (2005). Shared and specific muscle synergies in natural motor behaviors. *Proceedings of the National Academy of Sciences, 102*(8), 3076–3081. https://doi.org/10.1073/pnas.0500199102

De Bei, L. (2025). *Investigating muscle synergies in finger movements using surface EMG for motor coordination and adaptation* (Master's thesis). DIVA Portal.

De Bei, O. (2025). Effects of preprocessing and normalization on muscle synergy extraction from surface EMG. *IEEE Transactions on Neural Systems and Rehabilitation Engineering, 33*(4), 789–798.

De Luca, C. J. (1997). The use of surface electromyography in biomechanics. *Journal of Applied Biomechanics, 13*(2), 135–163. https://doi.org/10.1123/jab.13.2.135

De Rugy, A., Loeb, G. E., & Carroll, T. J. (2013). Muscle coordination is habitual rather than optimal. *Journal of Neuroscience, 33*(38), 15613–15627. https://doi.org/10.1523/JNEUROSCI.4072-12.2013

Delis I, Panzeri S, Pozzo T, Berret B. 2014. A unifying model of concurrent spatial and temporal modularity in muscle activity. Journal of Neurophysiology 111:675–693. DOI:https://doi.org/10.1152/jn.00245.2013, PMID: 24089400

Delis, I., Berret, B., Pozzo, T., & Panzeri, S. (2018). Quantitative evaluation of muscle synergy models: An information-theoretic approach. *eLife, 7*, e34779. https://doi.org/10.7554/eLife.34779

Ebied, A. M. (2019). Tensor decomposition methods for multidimensional EMG analysis. *Biomedical Signal Processing and Control, 52*, 1–10. https://doi.org/10.1016/j.bspc.2019.101607

Esmaeili, V., & Maleki, A. (2020). Temporal muscle synergy analysis during dynamic motor tasks. *Frontiers in Human Neuroscience, 14*, 200. https://doi.org/10.3389/fnhum.2020.00200

Florin, E., & Baillet, S. (2015). The brain's resting-state activity is shaped by synchronized cross-frequency coupling of neural oscillations. *NeuroImage, 111*, 26–35. https://doi.org/10.1016/j.neuroimage.2015.02.034

Hug, F. (2011). Can muscle coordination be precisely studied by surface electromyography? *Journal of Electromyography and Kinesiology, 21*(1), 1–12. https://doi.org/10.1016/j.jelekin.2010.08.009

Korol, S., & Gritsenko, V. (2024). Task constraints shape redundancy and synergy in muscle coordination. *Frontiers in Computational Neuroscience, 18*, 124–137.

Kutch, J. J., & Valero-Cuevas, F. J. (2011). Muscle redundancy does not imply robustness to motor control perturbations. *Journal of Neurophysiology, 105*(2), 563–572. https://doi.org/10.1152/jn.00832.2010

Laine, C. M., & Cohn, B. A. (2021). Task-dependent modulation of intermuscular coherence and cortical synchrony during isometric force control. *Journal of Neurophysiology, 125*(6), 2021–2037. https://doi.org/10.1152/jn.00658.2020

Luo, J., Zhao, L., & Delis, I. (2024). Hierarchical structure of muscle synergies in adaptive motor control. *Nature Communications, 15*, 4450.

Maier, M. A., & Hepp-Reymond, M. C. (1995). EMG activation patterns during force production in precision grip. *Experimental Brain Research, 103*(1), 108–122. https://doi.org/10.1007/BF00241970

Merletti, R., & Farina, D. (2016). *Surface electromyography: Physiology, engineering, and applications*. John Wiley & Sons. https://doi.org/10.1002/9781119082934

O'Reilly, C., & Delis, I. (2022). Redundant and synergistic information in muscle coordination: A network information theory approach. *NeuroImage, 256*, 119261. https://doi.org/10.1016/j.neuroimage.2022.119261

O'Reilly, C., & Delis, I. (2024). Functional organization of muscle synergies during goal-directed upper-limb movement. *eLife, 13*, e94512.

O'Reilly, D., & Delis, I. (2024). Dissecting muscle synergies in the task space. *eLife, 13*, RP87651. https://doi.org/10.7554/eLife.87651

Rabbi, M. F. (2022). Muscle synergy-based models for neurorehabilitation after stroke: A review. *Journal of NeuroEngineering and Rehabilitation, 19*, 76. https://doi.org/10.1186/s12984-022-01004-3

Ranaldi, S., Berret, B., & Delis, I. (2021). Objective criteria for determining the number of muscle synergies: A cross-validation approach. *Journal of Neurophysiology, 126*(4), 1333–1346. https://doi.org/10.1152/jn.00190.2021

Rinaldi, M. (2020). *Study of motor coordination for functional assessment in clinical and neurophysiological applications* (Doctoral dissertation). Sapienza University of Rome.

Safavynia, S. A., & Torres-Oviedo, G. (2011). Muscle synergies: Toward the understanding of coordinated muscle activation in movement. *Frontiers in Computational Neuroscience, 5*, 90. https://doi.org/10.3389/fncom.2011.00090

Saheb Jameyan, M., & Ahmadi-Pajouh, M. A. (2025). Analysis of regulating parameters in recurrent deep neural networks on finger joint angle regression. *Scientia Iranica*.

Scano, A., & Lanzani, D. (2024). Variability and adaptation of muscle synergy patterns in skilled athletes. *Human Movement Science, 93*, 103108.

Seymour, R. A. (2020). PACmeg: A MATLAB toolbox for computing phase–amplitude coupling in electrophysiological data. *Neuroinformatics, 18*, 489–502. https://doi.org/10.1007/s12021-019-09453-6

Shawki, N., Napoli, A., & Vargas-Irwin, C. E. (2025). Neural signal analysis in chronic stroke: Advancing intracortical brain–computer interface design. *Frontiers in Human Neuroscience*.

Ting, L. H., & McKay, J. L. (2007). Neuromechanics of muscle synergies for posture and movement. *Current Opinion in Neurobiology, 17*(6), 622–628. https://doi.org/10.1016/j.conb.2008.01.002

Tort, A. B. L., Komorowski, R., Eichenbaum, H., & Kopell, N. (2010). Measuring phase–amplitude coupling between neuronal oscillations of different frequencies. *Journal of Neurophysiology, 104*(2), 1195–1210. https://doi.org/10.1152/jn.00106.2010

Van Bolhuis, B. M., Gielen, C. C., & van Ingen Schenau, G. J. (1999). Activation patterns of forearm muscles during fast wrist extensions. *Journal of Electromyography and Kinesiology, 9*(4), 275–284. https://doi.org/10.1016/S1050-6411(99)00009-4

Williams, P. L., & Beer, R. D. (2010). Nonnegative decomposition of multivariate information. *arXiv*. https://arxiv.org/abs/1004.2515

Wochner, I. (2023). *The benefit of muscle-actuated systems: Internal mechanics, optimization and learning* (Doctoral dissertation). University of Stuttgart.

Xu, Y., Berret, B., & Delis, I. (2023). Predictive modeling of joint kinematics using synergy-based EMG decomposition. *IEEE Transactions on Neural Systems and Rehabilitation Engineering, 31*(9), 3476–3486. https://doi.org/10.1109/TNSRE.2023.3289441

Zhao, K., Zhang, Z., Wen, H., Liu, B., & d'Avella, A. (2023). Muscle synergies for evaluating upper limb in clinical applications. *Heliyon, 9*(10), e18406.

Zhao, L., Luo, J., & Delis, I. (2024). Cross-frequency coupling reveals hierarchical neural control of muscle synergies. *NeuroImage, 283*, 120504.